Annu. Rev. Fluid Mech. 2000. 32:573–611

VAPOR EXPLOSIONS

Georges Berthoud
Commissariat à l'Energie Atomique, Grenoble, Grenoble cedex 9, France, 38054; e-mail: georges.berthoud@cea.fr

Key Words nuclear safety, severe accident, multiphase thermalhydraulics, fuel coolant interaction

■ **Abstract** A vapor explosion results from the rapid and intense heat transfer that may follow contact between a hot liquid and a cold, more volatile one. Because it can happen during severe-accident sequences of a nuclear power plan, that is, when a large part of the core is molten, vapor explosions have been widely studied. The different sequences of a vapor explosion are presented, including premixing, triggering, propagation, and expansion. Typical experimental results are also analyzed to understand the involved physics. Then the different physics involved in the sequences are addressed, as well as the present experimental program.

1. INTRODUCTION

Vapor explosions are a subclass of what are called fuel coolant interactions (FCIs) in safety studies of nuclear reactors. An FCI involves all of the phenomena occurring after the contact of a hot liquid (the fuel) with a colder, more volatile liquid (the coolant). In vapor explosions (sometimes called energetic FCIs), heat transfer between the melt and the coolant is so intense and rapid that the timescale for heat transfer is shorter than the timescale for pressure relief. This can lead to the formation of shock waves and/or the production of missiles at later times, during the expansion of coolant vapor, that may endanger surrounding structures. In nuclear plants, there is then a risk of release of radioactive fission products into the environment, which is the reason that these phenomena have been widely analyzed during nuclear-safety studies.[1]

The term vapor explosion [sometimes called steam explosion (SE)] can be misleading, because the expanding fluid seems to be in a thermodynamic vapor state. But, in energetic FCIs, temperature and pressure can exceed their critical values. In such cases, the supercritical coolant can appear as a dense gas, and its rapid expansion can also be explosive.

[1]*Note to Readers*
The references in this article are numbered by order of appearance and cited by number in the text.

In the nuclear-energy industry, several energetic FCIs have occurred in test reactors; they are briefly summarized by Cronenberg & Benz (1). The first one occurred in 1952 in the Canadian NRX test reactor, and it was induced by the failure of the shutdown rod system, leading to fuel melting followed by the failure of the calendria tubes after a uranium-water interaction. Following this incident, a destructive reactor experiment was performed in the BORAX boiling-water-reactor test in 1954. In this test, most of the fuel plates melted during the power excursion, and, after the metal-water contact, the reactor tank was ruptured by a pressure peak that was estimated to be >40 MPa. Later, in 1961, it is thought that the withdrawal of a control rod in the stationary low power reactor 1 (SL1) boiling-water reactor led to a power excursion that disrupted the fuel elements into the surrounding water, causing a vapor explosion with a peak pressure estimated at 70 MPa. The pressure vessel rose 3 m after the shearing off of the pipings. Finally, in 1962, another destructive experiment was performed in the special power excursion reactor test-Idaho (SPERT) 1D test reactor, leading to a measured pressure of 27 MPa. It must be noted that all of these explosions resulted from reactivity excursions and that, in all cases, the fuel was metallic (U or U-Al alloy) and the coolant was water.

The only commercial nuclear plant ever damaged by an SE was Tchernobyl-4, in 1986. In this reactor, again, an uncontrolled power excursion led to the dispersion of fuel into the surrounding water, followed by one or two SEs that destroyed the reactor. These explosions dispersed the fuel and generated hydrogen.

Vapor explosions have also been reported in other industrial processes such as those used in foundries (steel and aluminum) and paper factories and in transport of liquid natural gas (LNG), during which hot fluid was brought into contact with some coolant (usually water). One of the last large explosions reported in a foundry occurred at the Appleby-Frodingham Steelworks in 1975 (2), where up to 90 tons of molten metal were thrown over a wide area after the contact of ≤2200 liters of water with 180 tons of molten metal contained in a torpedo. Damages were then mainly caused by heat transfer.

During the transportation of LNG, LNG (the coolant) can be spilled onto water (the hot liquid), leading to a vapor explosion—called "rapid phase transition" in this domain, which disperses the natural gas. In that case, we are concerned by the possibility of ignition and combustion during the mixing with air (3).

Fujii (4) reviewed the various geological conditions between magma and water (or wet sediments) leading to phreatomagmatic eruptions, to characterize the conditions of explosive interactions between magma and water beneath volcanoes. Fujii reported that some of the processes can be reasonably explained by FCI mechanisms.

Vapor explosions have also been observed with other systems of fluids. Buxton & Nelson (5) provide an exhaustive survey of hot-liquid–cold-liquid interactions based on materials that were available until February 1975.

During a vapor explosion, a hot liquid transfers its internal energy in a short timescale to a cold, more volatile liquid. This rapid heat transfer is caused by a fine fragmentation (FR) of the hot liquid, increasing drastically the interfacial area between the two liquids. The coolant temperature and pressure then increase, and the coolant expands, affecting the surroundings. The internal energy of the hot liquid is then partially transformed into mechanical energy. Evaluating the consequences of a vapor explosion involves calculating the yield of this transformation. This can be done from a purely thermodynamic point of view or with a dynamic approach, by trying to describe all of the kinetics of the process.

2. THERMODYNAMIC EVALUATION OF A VAPOR EXPLOSION

Thermodynamic evaluation of a vapor explosion was first reported by Hicks & Menzies (6), who estimated the maximum work potential available when a mass of fuel M_f at temperature T_f interacts with a mass of coolant M_c at temperature T_c. This gave an upper bound for the work potential of an explosion. To accomplish this, Hicks & Menzies considered the vapor explosion to be ideally composed of two steps, (*a*) a constant-volume, ideal mixing (i.e. instantaneous and without heat losses) of the two materials leading to temperature equilibrium and to a high-equilibrium pressure for the mixture and (*b*) an isentropic expansion of the mixture in which the temperature equilibrium is maintained.

To perform their calculations, Hicks & Menzies (6) made additional simplifying hypotheses, that is:

1. Liquids are incompressible, and their specific volumes are negligible when compared with those of vapor;
2. Vapor is considered a perfect gas;
3. Specific and latent heats are kept constant.

Later, many others made the same types of calculations, while relaxing some of the hypotheses, mainly by improving the equations of state (see 7:57). An example of such a calculation is shown in Figure 1 for a melt prototypical of a hypothetical core melt accident in a pressurized-water reactor. This figure summarizes the efficiency η of the transformation of the internal energy ΔE of the melt into the mechanical energy of water coolant as a function of the ratio volume of coolant/volume of melt, implied in the vapor explosion. This calculation shows that $\sim$50% of the melt internal energy can be transformed into mechanical energy if equal volumes of melt and coolant interact. Moreover, the efficiency is $>$10% for a wide range of volume ratios. Because tons of fuel might be molten in a hypothetical core meltdown accident, mechanical energy in the gigajoule range can then be obtained. Such estimates triggered the study of vapor explosions to

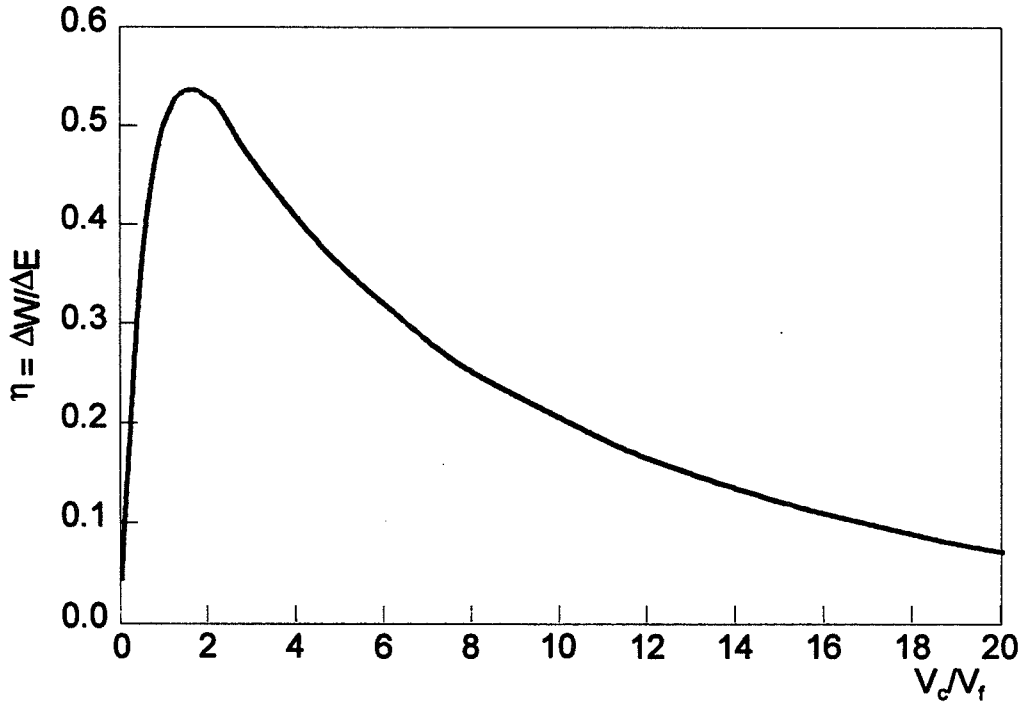

Figure 1 Efficiency of a corium-water interaction based on the Hicks-Menzies hypothesis. Corium at 3000 K UO_2, 54% (mass); Zr, 16%; Fe, 25.5%; Cr, 3%; Ni, 1%; ΔE = 1647 kJ/kg available internal energy in the melt.

get more realistic figures for the assessment of nuclear-plant safety. Experimental and analytical programs were launched to understand the explosiveness of a melt under a variety of conditions, to quantify conversion ratios of vapor explosions, and to understand the effect of scale on vapor explosion phenomena (i.e. what happens with larger masses?). After 10 years, a large body of experimental data was obtained on the behavior of a small amount of hot liquid in contact with a vaporizable coolant. Generally, low energy yields (on the order of 1% of the internal melt energy) were obtained even though fine fragmentation of the hot material was observed. These results are summarized by Cronenberg & Grolmes (8). It was then felt that, to get information on the energetics of vapor explosions, there was a need for larger experiments. This was done in particular in the THERMIR experiment in Winfrich (9), in which $\leq$20 kg of molten tin or aluminum were poured into a tank filled with water. High-speed movies (5000 images per second) showed that, when an interaction was observed, it usually started at the chamber base after a coarse melt dispersion was obtained in the lower half of the tank in $\sim$1 s. Then, the interaction front propagated at $\sim$200 m/s through the coarse mixture. Pressures of $\leq$40 MPa were measured, and efficiencies of $\sim$10% of the thermodynamic maximum one were estimated. This led Board & Hall (10) to subdivide the vapor explosion process into four steps, which are now well recognized in the FCI community.

3. GENERAL DESCRIPTION OF THE STEAM EXPLOSION PROCESS

From their observations of the phenomena occurring in large-scale experiments (~20 kg of melt), Board & Hall proposed four phases to describe a SE.

3.1. The Premixing Phase

Board & Hall (10) described the formation of a premixed or coarsely mixed region as " . . . the setting up of a quasistable initial configuration." In this phase, as soon as the two liquids meet, a stable vapor film allows large quantities of melt and coolant to intermix owing to density and/or velocity differences as well as vapor production. In fact, the vapor film causes relatively low heat transfer between the two liquids, which corresponds to a quasistable or metastable state called the premixing phase. The timescale is in the range of seconds, and the length scale is in the range of centimeters (i.e. the melt is progressively fragmented into particles of centimeter-scale size).

3.2 The Triggering Phase

The triggering phase of this configuration leads to some local fine FR and then enhanced heat transfer and pressurization. The triggering event is something that produces the destabilization of the vapor film, allowing liquid-liquid contacts. Many mechanisms may be responsible for this destabilization, including pressure pulses resulting from impact (interactions are often triggered when the melt reaches the bottom of the tank), thermal film destabilization, and coolant entrapment within the melt.

3.3 The Propagation Phase

During the propagation phase, there is an escalation process resulting from the coupling between pressure wave propagation, fine FR, and heat transfer after the trigger event. It is thought that the pressurization induced by the trigger destabilizes the surrounding vapor films, leading to the fine FR of the surrounding melt. Early in this process (when the induced pressure is not too high), it is thought that fine FR results from local liquid-liquid contacts after the vapor film destabilization. Locally, some coolant is rapidly heated and pressurized, and this causes some fine FR of the surrounding melt. This type of fine FR is often called "thermal fragmentation." Then, when the pressure is high, the fine FR is believed to be of a hydrodynamic nature owing to the relative motion between the melt and the coolant induced by their different densities and compressibilities.

3.4 The Expansion Phase

The expansion of the resulting high-pressure mixture behind the propagation front against the inertial constraints imposed by the surroundings determines the damage potential of a vapor explosion. In fact, if the locally high pressures (the

propagating shock) are quickly relieved, then they may not damage the surrounding structures, but the kinetic energy transmitted to the materials around the interaction zone may be the damaging agent.

3.5 Other Modes of Contact

It must be recognized that the four-phase description was deduced from experiments in which the hot fluid, which was also the denser one, was poured into the cold one, which is the most important mode of contact for nuclear-safety studies. But other modes of contact between hot liquids and coolants can occur: (*a*) coolant may be poured onto the hot liquid; (*b*) coolant may be injected under pressure into the hot liquid; and (*c*) coolant may be layered on the hot liquid, in a stratified mode of contact.

When coolant is trapped into the melt, it may reach very high degrees of superheat [up to spontaneous nucleation (12)], and then very high pressure during flashing. But, in such cases, the energetics of explosion are limited by the amount of coolant that can be mixed with the hot liquid (mixing is much more difficult in this situation).

As for the stratified mode of contact, there is no premixing phase, but it is believed that the propagation of the pressure wave is responsible for the mixing and FR of the two liquids.

Another exception to the above-described four-phase SE is the reactivity-initiated accident that occurred in the BORAX, SL1, and Tchernobyl 4 reactors, in which a nuclear-power excursion led to a fine dispersion of the liquid fuel, by the high-pressure-fission gases or fuel vapor, into the liquid coolant. This was well described by El Genk (13) in his analysis of the in-pile reactivity initiated accident (RIAST 4) experiment.

From their observations of the explosions obtained in the THERMIR facility, Board et al (11) also proposed an analogy between a chemical detonation and a vapor explosion, which was then called a thermal detonation. In a chemical detonation (14), a shock wave goes through the inert reactants, compresses them, and increases their temperature, which causes rapid chemical reactions to occur in a short region behind the shock front (the reaction zone). For a 1D steady-state detonation, the classical jump conditions for shock waves apply. For example, in the shock-front frame of reference, we have

$$\rho_1 V_1 = \rho_2 V_2 = G, \tag{1}$$

$$p_1 + \rho_1 V_1^2 = p_2 + \rho_2 V_2^2, \tag{2}$$

$$E_2 - E_1 = \frac{1}{2}(p_1 + p_2)(v_1 - v_2), \tag{3}$$

where index 1 indicates unreacted material before the shock front; 2 is after the reaction is completed; $\rho = 1/v$ = density of the mixture; p = pressure in the mixture; V = velocity of the mixture; and $E(p, v)$ = internal energy of the mixture.

In that case, Equation 3 gives all the possible states of detonation and is called the adiabatic of detonation or the Crussard curve (the thick curve in Figure 2b), although, if the jump conditions are applied just through the shock (i.e. index 2 would correspond to the adiabatically compressed reactants without any reactions), Equation 3 would give all the possible states after a shock in an inert medium. These states are located on the shock adiabatic or Hugoniot curve (the *dashed curve* in Figure 2b).

From Equations 1 and 2, we have $G = [(p_2 - p_1)/(v_1 - v_2)]^{1/2}$, which shows that all of the possible states of detonation are on the Rayleigh line, which is issued from the pole X (p_1, v_1) with a slope equal to G^2 through the detonation wave.

It can then be shown (14) that the only possible stable steady state is obtained when the Rayleigh line is in tangent with the adiabatic of detonation. This determines the Chapman-Jouguet (CJ) point (0 in Figure 2b). At this point, the velocity V_2 of the material (in the shock-front frame) is equal to the sound velocity, so rarefaction waves from the expansion region after the CJ point cannot penetrate the reaction zone.

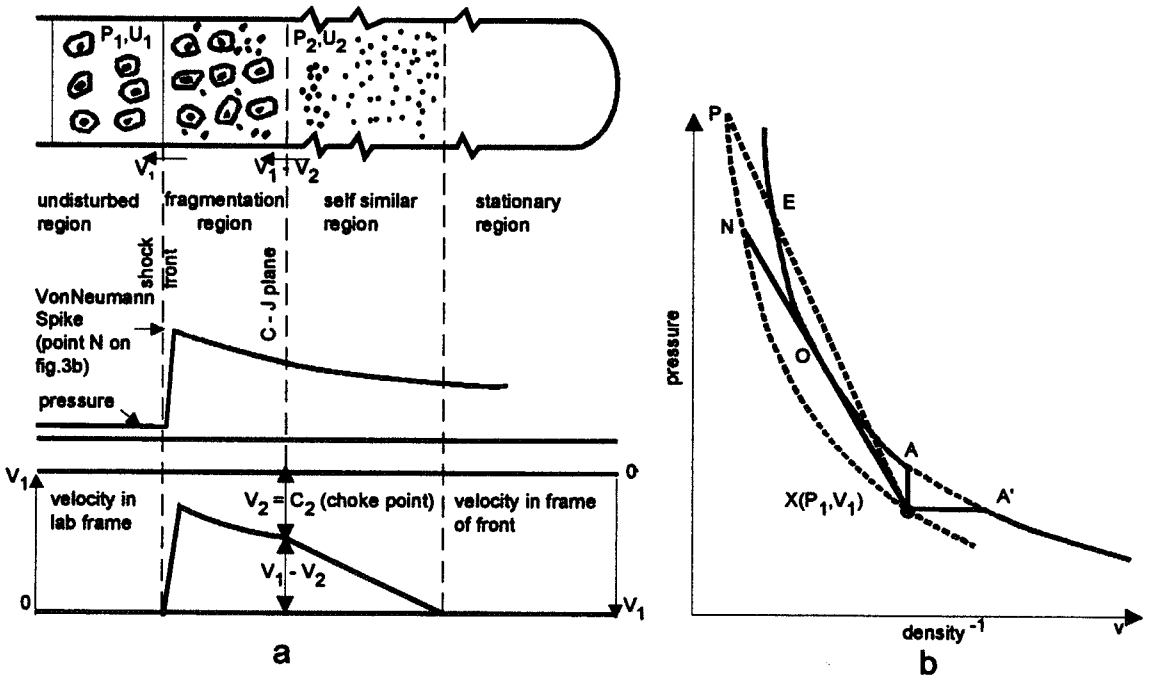

Figure 2 (a) Geometry and schematic pressure and velocity profiles of a 1D explosion; (b) Schematic shock adiabatic (solid curve, reacted material; dashed curve, unreacted material) (from 14).

The schematic description of a steady-state chemical detonation is therefore the following. A shock wave goes through the inert indium, which is pressurized up to the Von Neumann point (*N* in Figure 2b). Then chemical reactions start, and the pressure falls up to the CJ point at the end of the reaction zone. Behind the reaction zone, the pressure falls based on the far-field conditions.

In their analogy, Board et al (11) described (*a*) the metastable premixture as the unreacted material in which (*b*) a shock wave propagates, increasing the pressure up to the Von Neumann point for a chemical detonation. (*c*) This pressure wave collapses the vapor film, and owing to the density difference, induces large relative velocities between the fuel drops and the surrounding liquid. These velocity differences entrain fine FR and rapid heat transfer. This occurs in the FR region (the reaction zone for an explosive). (*d*) Then a steady state may be reached, if the energy release is large enough to sustain the shock propagation. So they applied Equation 3 to build adiabatic detonation curves, for a UO_2-Na system, for example, assuming complete reaction; that is, at the end of the reaction zone, the melt and the coolant are in thermal and mechanical equilibrium. In doing so, Board et al (11) obtained very high pressures, on the kilobar scale, as can be seen in Figure 3b.

This concept was then extended to include the facts that (*a*) all of the melt may not be fragmented so that only part of it may come in equilibrium with the coolant (15–16) (see Figure 3b), and (*b*) all of the coolant may not be involved in the rapid heat transfer process (17).

To test this concept, Scott & Berthoud (15–16), rapidly followed by Sharon & Bankoff (18), provided the first multiphase-flow modeling of a steady-state thermal detonation. In their model, they described the FR induced by the shock wave and assumed that, owing to the fragment size and the turbulence in the interaction zone, the fragments came instantaneously into thermal and mechanical equilibrium with the coolant; then these researchers looked for the existence of a CJ plane. An example of such a mechanistic calculation is given in Figure 3a, which shows the behavior of the two components (large melt drops and debris coolant mixture) in the reaction zone after the shock wave in a self-sustained thermal detonation. Such a self-sustained state is not obtained in any case, and, of a given premixture (*X* point in Figure 2) and for a given FR model, there is only one shock wave that can lead to steady-state propagation. To check the validity of the two-component model, they also performed thermodynamic calculations of the CJ states from the adiabatic detonation curves built through the classical detonation relations (Equations 1 and 3), using the percentage of FR of melt included in the interaction as a parameter.

The CJ states are obtained through the classical tangency condition and are represented by the *thick line* in Figure 3b. In Figure 3b, the thermodynamically calculated CJ state for the conditions given in Figure 3a corresponds to a degree of FR between 0.35 and 0.40, which is in agreement with the value obtained by the model (see Figure 3a).

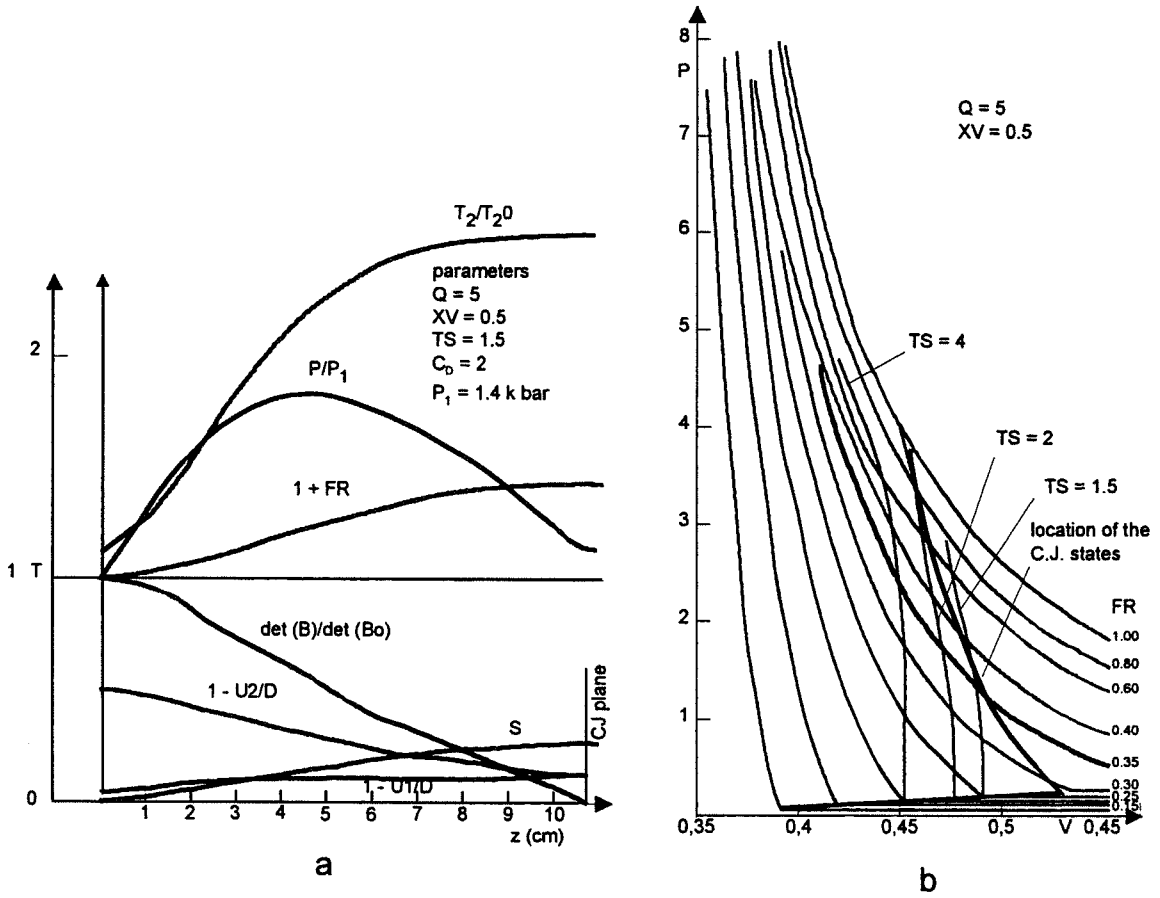

Figure 3 (a) Evolution of components velocities and temperature, of pressure and degree of fragmentation (FR) for a UO_2-Na mixture behind a 1.4-kbar shock wave (Q) = mass ratio of melt to coolant, XV = initial void fraction, TS = breakup time constant, C_D = drag coefficient, D = shock wave propagative velocity; (b) possible states of detonation in a PV diagram for the above premixture based on the fragmentation degree FR (from 16).

4. EVALUATION OF THE CONSEQUENCES OF A VAPOR EXPLOSION

To quantify the consequences of an SE, it is necessary to estimate (*a*) the transient pressure loads on the structures, which correspond to the early (~1–10 ms) effect of an SE, that is, the result of the propagation phase, and (*b*) the mechanical energy of the expanding IZ, which is transformed into kinetic energy in the surrounding medium during the expansion phase (~10–100 ms).

Because the thermodynamic (Hicks & Menzies or Board & Hall) estimations give very high values, it became necessary to provide more realistic values. This was done during the 1970s by the development of lumped parametric models and more recently by the development of multidimensional multifield mechanistic

codes, as well as by means of experimental programs with melt masses from 1 g to ~20 kg at maximum.

In the lumped parametric models, some kinetics were provided for the mixing-FR processes as well as for heat transfer. One of the first models, which can be taken as a reference for all the others, was proposed by Cho et al (19). In this model, they described the transient evolution of the coolant in the interaction zone (IZ), which receives heat from the fuel and expands against acoustic and inertial constraints (see Figure 4). They did not assume instantaneous thermal equilibrium, but used a heat transfer time constant t_h, and did not assume instantaneous mixing, instead describing the progressive FR and mixing of the fuel within the coolant with another time constant t_m. The final heat transfer rate from fuel to coolant was then

$$\frac{dQ}{dt} = \frac{C_f M_f}{t_h}\left(\sqrt{\frac{3t_h}{nt}} + 1\right)\left[1 - \exp\left(\frac{-t}{t_m}\right)\right](T_f - T_c),$$

where t_h = heat transfer time constant $= R_f^2/3\alpha_f$ (controlled by conduction within the fuel), and R_f = radius of fuel particles after fine FR and C_f, and α_f = thermal capacity and diffusivity of the fuel.

By using this law, the progressive evolution of the interfacial area between fuel and coolant is described as $A(t) = A_\infty\,[1 - \exp(-t/t_m)]$ with $A_\infty = 3\,M_f/\rho_f R_f$ being the final interfacial area. This does not represent any particular FR mechanism, but it is an easy way to describe the progressive FR and mixing of the fuel within the coolant. With such a model, it is then possible to calculate the pressure time history and the mechanical-energy delivery law.

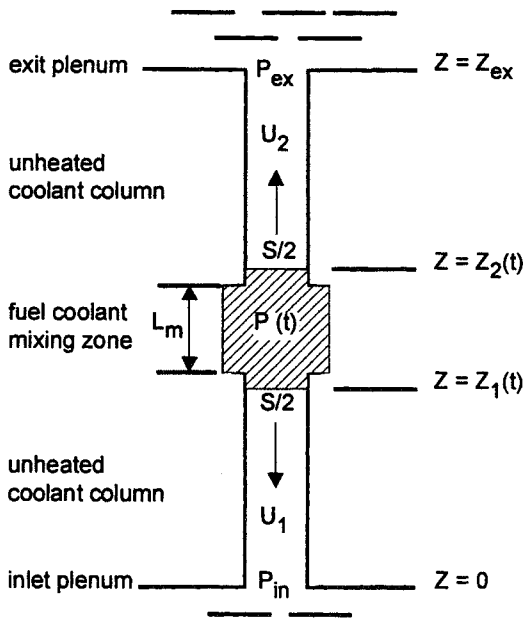

Figure 4 The system described by Cho et al (from 19).

During the 10 years after the publication of the model by Cho et al (19), a lot of parametric models were built by following the same approach; that is, the IZ was considered as a whole, expanding against the surroundings. These models were summarized in the review by Corradini et al (7). Improvements in these later models include (*a*) better description of the fuel-coolant heat transfer, (*b*) entrainment of cold coolant in the IZ by instabilities occurring during early expansion, (*c*) heat transfer to structures, (*d*) mechanistic description of the FR based on the physics being considered, and (*e*) the presence of noncondensable gases.

Such a model, developed by Berthoud & Newman (19a), allowed an interpretation of the results obtained in the CORECT 2 facility. In this facility, 100 liters of Na were brought into contact with 5 kg of molten UO_2. The observed FCIs were recalculated by the parametric code URANUS, which uses the Cho et al approach in its simplest version or an FR model based on the thermal FR of the fuel solid crust in its most elaborate version.

With this model, two steps were identified in the FCI process:

1. A phase during which the pressure rises in the IZ, owing to the very high heat transfer resulting from the fine FR. In this phase, the thermodynamic conditions of the coolant are very important, whereas the overall system is of secondary importance (corresponding to the instantaneous-mixing and thermal-equilibrium phase of Hicks & Menzies).
2. The expansion phase, which is system dependent. During this phase, heat transfer from the IZ to the surroundings by entrainment or condensation on structures replaces heat transfer from fuel to coolant (corresponding to the isentropic-expansion phase of Hicks & Menzies).

To illustrate this model, we briefly present the results of a calculation of the most violent explosion obtained in CORECT 2. In this calculation, 30 ms after the beginning of the interaction, the maximum pressure is reached in the IZ, which contains ~1 kg of low-quality ($x = 0.5 \times 10^{-5}$) sodium at 1915 K. At this time, the coolant has received 1.6 MJ from the fuel and has transferred 0.3 MJ to the structures, the delivered mechanical energy being only 2 kJ. At the end of the expansion, 250 ms later, there are ~4 kg of Na at 1240 K in a two-phase state ($x = 0.34 \times 10^{-2}$). In the IZ, the fuel has lost 0.7 MJ more, whereas the heat losses are 0.86 MJ and the mechanical-work is 24 kJ.

This shows that, because the parameters used to describe the vapor explosion have an influence mainly during the first phase, which is not very system dependent, we may use these parameters with some confidence in other situations. However, such a description does not really follow the description of the four phases of a large-scale vapor explosion (LSE) previously detailed. The premixing phase is not described but prescribed as an initial condition for calculating the explosion itself. The explosion does not propagate through the mixture, but starts everywhere at the same time in the IZ, even if the fuel is progressively more involved in the interaction process.

5. EXPERIMENTAL VAPOR EXPLOSION PROGRAMS

By the time the parametric models were built, estimations of SE consequences were also addressed from an experimental point of view. Experiments were carried out to understand the explosivity of a melt. These experiments examined the conditions in which a spontaneous explosion occurred when the two liquids were brought into contact (in different ways) or examined the conditions that can lead to a triggered explosion (using an external cause to destabilize the vapor film around the melt, such as pressure disturbances, cold-liquid injection, and so forth).

Other experiments were performed to quantify the effects of an SE in terms of pressure peaks; that is, rise time, maximum pressure, pulse width, and conversion ratio (η) that is, how much of the internal energy of the melt is transformed into mechanical energy. This quantity is then used to evaluate the mechanical energy release in an SE if we are able to evaluate the amount of melt involved (M_c) in the SE by $\Delta W = \eta M_c \Delta E$ (ΔE = available thermal energy in the melt).

Because the determination of this mass M_c is part of the SE problem, most of the experimentally evaluated conversion rates use the total mass of melt ($M_{c\infty}$) that is brought into contact with the coolant; that is, $\Delta W = \eta_\infty M_{c\infty} \Delta E$. These experiments also examine (*a*) the effect of scale and constraints on the above quantities, that is, how the peak pressure, the conversion ratio, and other factors evolve when larger masses of liquids are used and/or when the constraint imposed by the surrounding medium is varied; and (*b*) the effect of the contact mode, for example, pouring, injection, entrapment, stratified contact, and so forth.

A rather important experimental program has been performed and cannot be fully addressed in this paper. Detailed information can be found in the review papers of Berthoud (20), Corradini et al (7), and Fletcher (21). This experimental program can be subdivided by the mass of melt: (*a*) small-scale experiments use melt mass of some grams and generally use one melt drop. They are very important because they allow a better control of the experimental parameters, as well as the reproducibility of the experimental results. The experimental parameters include the melt composition, temperature and mass, nature and temperature of the coolant, ambient pressure, type and energy of the external trigger (if any), and mode of contact. (*b*) Larger-scale experiments use kilogram-scale masses (1–20 kg) of melt. These experiments, less numerous owing to their costs, are used to see how the conclusions drawn from the small-scale programs extend to larger masses (scale effect) and how the loop geometry influences the results (the constraint effect).

Among all of the experiments performed (see the list in 7), only information from the programs carried out at Sandia National Laboratory (SNL) (U.S.A.) and Winfrith (U.K.) is presented, because these programs covered most of the studied problems.

5.1 The Sandia National Laboratory Experimental Program (22–34a)

Both small- and large-scale experiments have been carried out.

5.1.1 Small Scale Program Two different devices were used to study the influence of the mode of contact. In one experiment (see Figure 5) ~10 g of melt were placed in a crucible. Then a retractable sleeve allowed some water to flood the melt. In this experiment, two types of trigger were used—an explosive wire, giving pressures of about 1 MPa and a 50-μs duration, and a minidetonator developing pressure of ≤10 MPa.

In another experiment (Figure 6), a melt drop (0.05–5 g) was dropped into a water tank, and the trigger (exploding wire) was activated when the drop, surrounded by a vapor film, was located in front of a high-speed camera.

From the high-speed movies, it was possible to describe the observed behavior of a single melt drop, initially surrounded by a vapor film and subjected to a pressure pulse. Just after the trigger, some hot spots appeared just outside a first expanding bubble. They corresponded to fine fragments of melt. In the flooded experiment, small jets of melt were ejected from the melt into the coolant. After

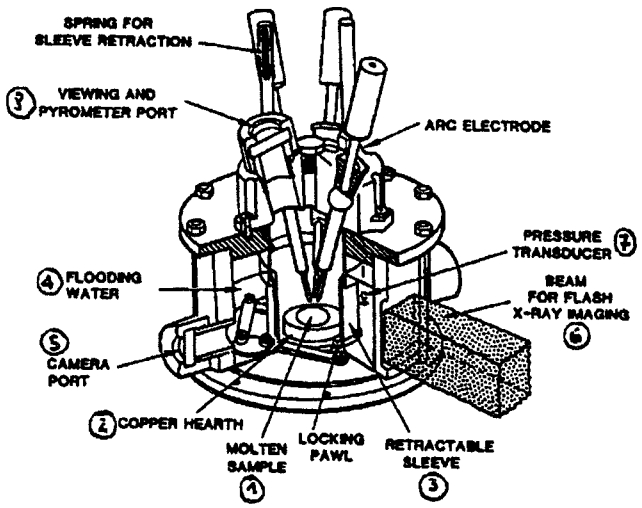

Figure 5 Cutaway drawing of floodable arc melter for steam explosion-triggering studies (from 25).

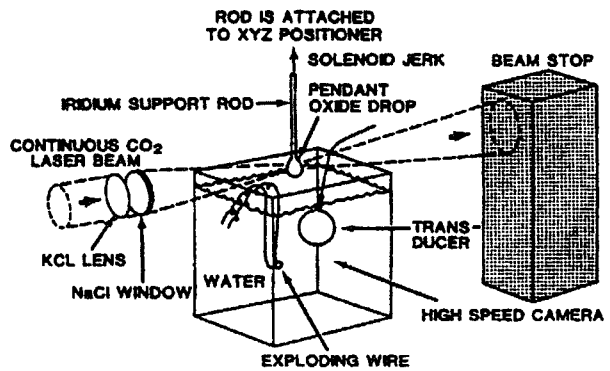

Figure 6 Drawing of the SNL single-drop experiment (26).

some expansion, the bubble started to collapse and, shortly after the collapse, small fragments of melt were again ejected. The vapor produced by these fragments when they contacted the surrounding cold liquid gave rise to a larger bubble, which again collapsed, leaving dark (i.e. cold) fragments outside the bubble. At this second collapse, if the drop was not yet completely fragmented, another expansion collapse cycle might start. Measurements of the evolution of the bubble radius and of the pressure close to the bubble illustrate this behavior, as can be seen in Figure 7.

The interaction is quantified by the maximum measured pressure peak, the work done by the expanding bubble (which can be estimated by the product of the ambient pressure P_∞ multiplied by the maximum bubble volume V_{max} (see

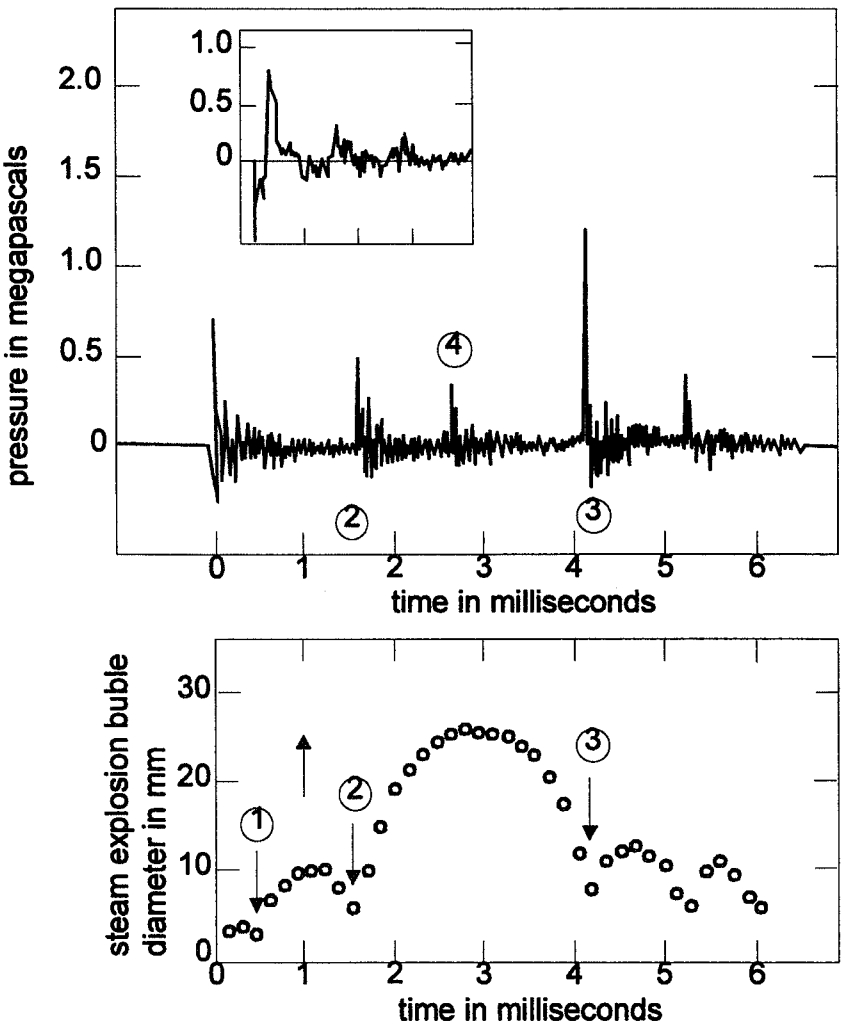

Figure 7 Pressure close to the bubble and bubble radius in a triggered single drop experiment. *1*, Vapor film collapse from the trigger pulse; *2*, 1st bubble collapse; *3*, 2nd bubble collapse; *4*, pressure peak associated with the collapse of the bubble created by the exploding wire at the bottom of the tank (Figure 6).

42), and the post mortem debris size, which is smaller when the explosion is larger. Observations of these debris show some larger, spherical fragments and a lot of smaller ones that are not spherical, as can be seen in Figure 8. These small particles do not have shapes typical of a fragmented solid but have rounded shapes. They are thought to be torn out of the liquid melt after liquid-liquid contacts after the vapor film or bubble collapses. Then, owing to their small size, they do not have time to become spherical before solidifying.

Results of the parametric studies can be summarized as follows:

1. Some melts did not lead to explosion. This was particularly true for metallic melts that produce H_2, which reinforces the stability of the vapor film. This was also true for any other reasons leading to the presence of noncondensable gases. This was also the case if the external part of the melt had time to solidify before the film destabilization (involving a long dwell time before spontaneous or triggered film collapse).
2. Explosions became less likely or could be suppressed when the coolant temperature approached saturation and when the ambient pressure increased. In both cases, this was explained by increased stability of the vapor film. It was also noted that an explosion at high ambient pressure had a similar behavior to that observed at atmospheric pressure but was more energetic (more fragmentation, and smaller fragments). This was explained by the fact that, at high pressure, the volume occupied by the produced vapor was less important, allowing more melt water contacts.
3. There was a definite effect of trigger strength. In a domain in which no explosions were observed for a given trigger, the use of a higher energetic trigger might lead to an explosion. Once again, this can be explained in terms of film stability. Thus it is important to use a realistic trigger in experiments, that is, to compare the trigger energy and the explosion energy. This is discussed by Henry (35).

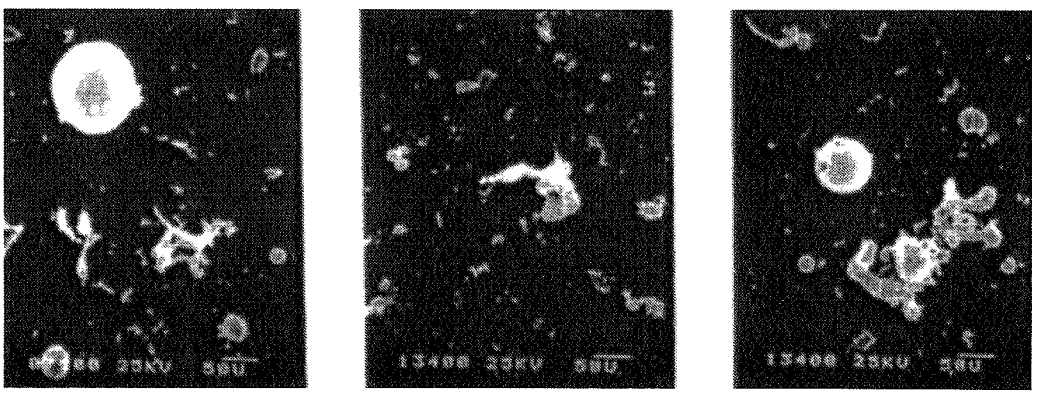

Figure 8 Debris from a iron oxide drop experiment (— = 50 μm) (from 26).

4. The melt temperature was not of primary importance when solidification of the external part of the melt was not especially important as it has been shown in some experiments (36).

Dullfore et al (37) performed another type of single-droplet experiment without using an external trigger, to evaluate the conditions in which a spontaneous explosion could occur. They defined the temperature IZ (TIZ), that is, the domain of the frame-of-reference initial melt temperature versus the initial coolant temperature, in which spontaneous explosions occurred. Such a TIZ is represented for tin and water in Figure 9.

Very clear boundaries were found, including (*a*) a horizontal boundary associated with coolant freezing; (*b*) a vertical boundary associated with melt freezing; and (*c*) a diagonal boundary associated with the stability of the vapor film; it was also observed that the closer the experimental point was to this diagonal boundary, the larger the dwell time (explosion time minus contact time).

Another explanation was also proposed to explain the occurrence of spontaneous explosions, based on the concept of "superheat limit" by Katz (12), later modified by Fauske (39, 40), who proposed the so-called Fauske criterion for an explosion to occur; that is, the instantaneous interface temperature (based on classical conduction calculations) must be larger than the spontaneous temperature of the coolant. It must be mentioned that, whereas this criterion is largely verified with small-scale experimental explosions, it has been invalidated for

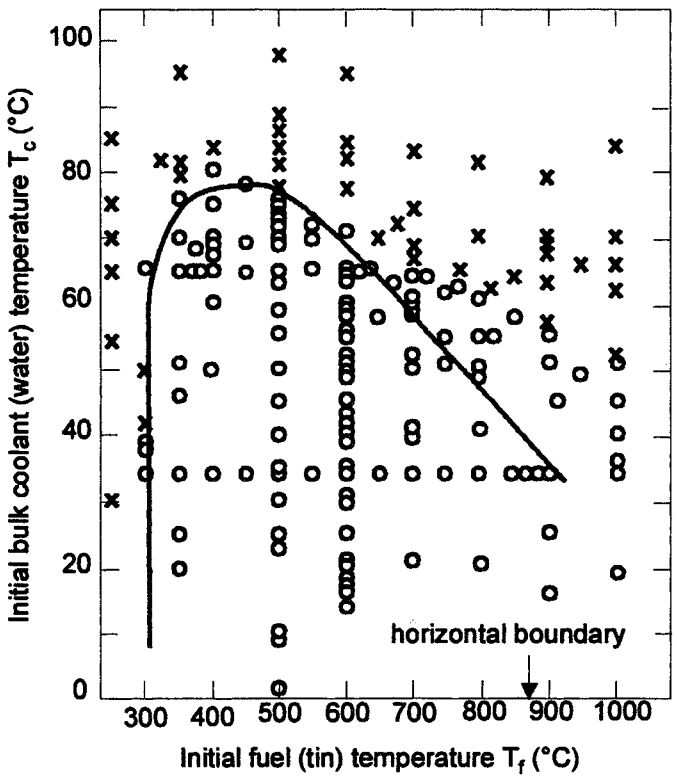

Figure 9 Temperature interaction zone for 12 g of tin dropped through 3 cm into boiled distilled water (from 37). o, interaction; x, no interaction.

large-scale experiments (see 19a, for example) in which the constraint allows long contact times between fuel and coolant and then allows them to build to an explosion.

It must also be mentioned that it is possible to trigger an interaction outside the TIZ by external actions like the application of a pressure pulse and that, once triggered, such an explosion is similar to a spontaneous one. These small-scale experiments helped clarify the basic processes of the fine FR occurring at the onset of an SE. They often used an external trigger. Then we had to understand the explosivity of a melt, that is, the likelihood of occurrence and the energetics of an SE. This can only be done by using large masses of melt and coolant, which are then quickly analyzed.

5.1.2 Large-scale Sandia Program At Sandia National Laboratories (SNL), an important experimental program involving melt at ~20 kg has been carried out in two different facilities. In an initial series of 60 scoping tests in an open-geometry experiment with minimum instrumentation, Al_2O_3-Fe thermite (an easy-to-get stimulant of corium) was used while, for 10 tests, a mixture of UO_2 (53% wt), ZrO_2 (17%), and SS (30%), called corium A + R, in pressurized-water-reactor safety was used. In this facility (see Figure 10), the mechanical work was estimated from the impulse delivered downward to the crushable honeycomb block and from the upward energy of the expelled melt and water.

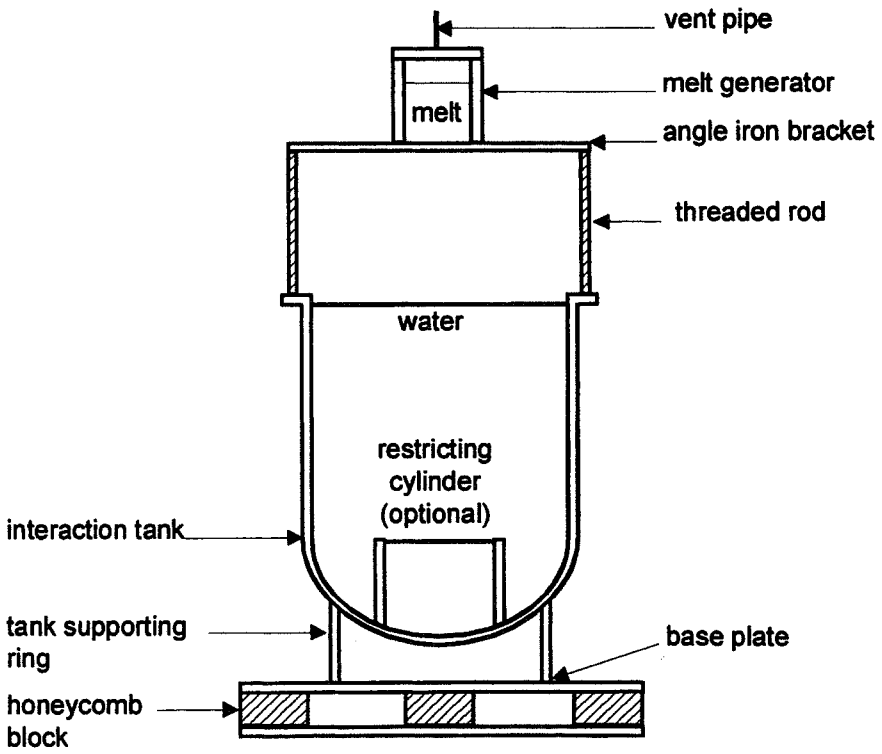

Figure 10 The open-geometry experiment.

In a second series to get more insights into the SE phenomena, the fully instrumented tests series (FITS) was performed, in which the explosion energy was more clearly measured as a function of melt composition, coolant subcooling, ambient pressure, and so forth. In this FITS series (see Figure 11), the melt was usually dropped into a plexiglas tank to allow visual observation of the processes. This tank was confined in a large, closed vessel in which measurements of the temperature and pressure of the cover gas were used to estimate the work done by the vapor on the compressible medium through the relation $\eta_D = (\Delta P \cdot V)/(\gamma - 1)\Delta E$, with ΔP being the pressure increase in the vessel, V the volume of the vessel, γ the ratio of specific heat, and ΔE the heat content of the melt.

From measurements of the velocity of the ejected materials and from estimates of their mass, it was possible to estimate their kinetic energy KE and to define a second efficiency $\eta_{KE} = KE/\Delta E$. Then, the total efficiency was taken as the sum of these two.

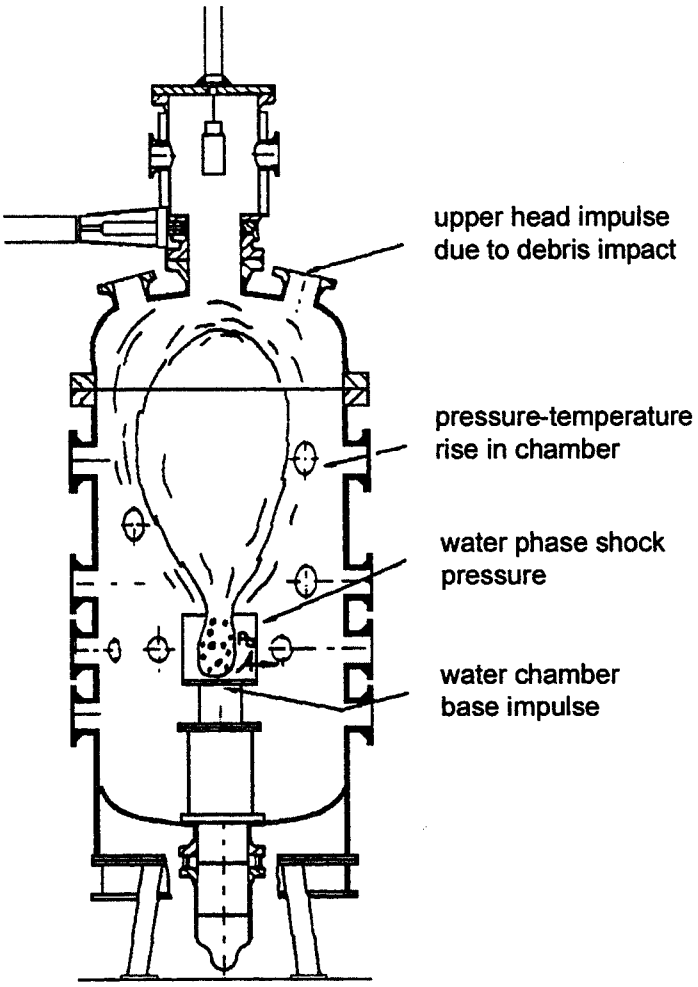

Figure 11 Sketch of the fully instrumented test series loop.

Other measurements included pressure traces and post-mortem debris analysis. Detailed analyses of these two experimental programs can be found elsewhere (22–34) and are summarized by Berthoud (20). They are briefly summarized here.

1. From the high-speed movies, the different phases of a SE were clearly recognized when the melt dispersed into the coolant (premixing), a spontaneous trigger occurred, and then the explosion propagated through the mixture.
2. The trigger often occurred when the melt hit the base of the tank, when the melt hit the free surface, or at any place during the dispersion.
3. The explosion showed many analogies with a chemical explosion. For example, the propagation velocity increased with the mixture density and with the width of the mixing zone. In addition, the mixture should not be too rich or too poor in fuel (chemical explosion shows a maximum efficiency for a given amount of oxygen), as can be seen in Figure 12.
4. There is a clear effect of melt composition on explosivity. In the open-geometry facility, most of the experiments with Al_2O_3-Fe thermite led to a spontaneous explosion (η_∞ from 0.2% to 3% of the total melt thermal energy), whereas no energetic explosions were obtained with corium A + R. In the FITS oxide melt series, Fe_xO_y was used to avoid the H_2 production observed with the thermite, which can inhibit the SE, explosions occurred regardless of the water subcooling, and they appeared more energetic than those observed in the Al_2O_3-Fe tests.
5. There is an effect of the coolant temperature. With the Al_2O_3-Fe thermite for example, the efficiency decreases when coolant temperature approaches saturation, and spontaneous explosion becomes less likely with saturated water.
6. There is an effect of ambient pressure. When the ambient pressure increases, a spontaneous explosion is less likely. But the use of an external trigger may

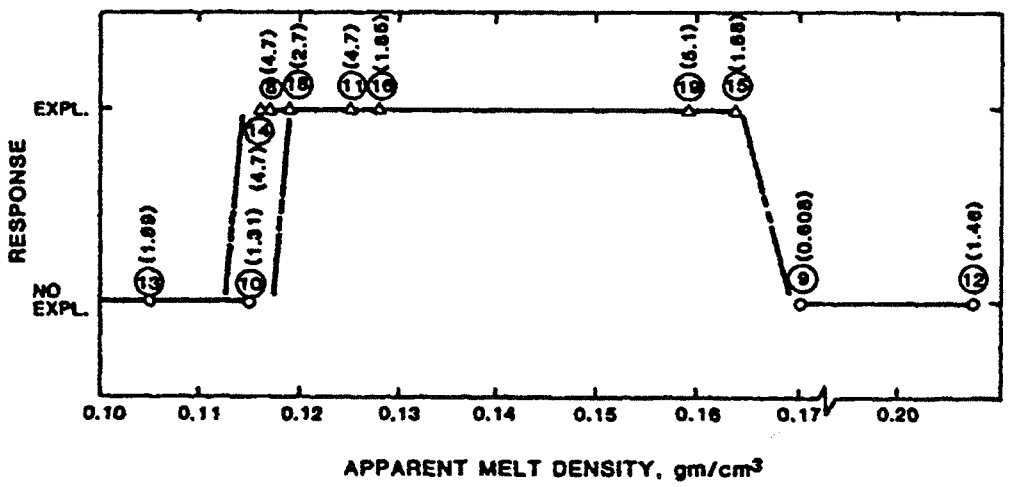

Figure 12 Melt explosivity as a function of the apparent density of the mixture (from 26).

allow us to observe an explosion in a domain in which no spontaneous explosion was previously observed. It has also been observed that SEs at high ambient pressure are more energetic (as for small-scale explosions).

These last two observations can be well explained in terms of ease of vapor film destabilization,

7. There is a scale effect. In the Al_2O_3-Fe open-geometry tests, no spontaneous explosion was observed for a melt mass of <2 kg, whereas with larger masses (~20 kg) in the FITS B series, for example, multiple explosions were sometimes observed. However, no clear conclusions could be drawn on the relationship between the efficiency and the scale, even if it could be postulated that efficiency should increase with scale. In fact, when an SE occurs in a system of size L, the energy transferred from melt to coolant is proportional to the IZ volume, that is L^3, whereas the losses are proportional to the external IZ surface, that is, L^2.
8. All of the melt mass is not involved in the SE process; that is, is found finely fragmented after the explosion (only the fine fragments have time to release their heat during the pressure buildup, i.e. the explosion time scale).
9. There is a constraint effect that was studied in the FITS Rigid Container (RC) test. In this test, Al_2O_3-Fe thermite was also used, but the usual plexiglas tank was replaced by a thick steel tank (500 kg). In test RC2, this led to a very violent explosion. Estimates of the conversion ratio from pressure traces, mass, and velocity of the ejected materials and from structural damages were reported by Berman et al (33) to be between 6% and 17% of the total melt thermal energy (owing to measurement uncertainties). This increase is easily explained if we consider that, with such a rigid wall, melt and coolant stay in contact and exchange heat longer, whereas, in the tests with the plexiglas tank, as soon as the pressure increases, as the walls are destroyed, melt and coolant are rapidly separated.

5.2 The Winfrith Experimental Program Using UO_2-Mo Thermite (41–43)

In Winfrith, a program using a UO_2-Mo (19% w) thermite source has been carried out to study the scale and constraint effects. In fact, in a first series of tests, 0.5 kg of thermite was released under water (from the thermite generator source under pressure of the gases produced at around 1 MPa) into a 52-liter tank filled with cold water and covered by argon (1.2 and 3.6 l). Later, a 24-kg source was used in a 1.7-m^3 tank (1500 kg of water and about 250 liters of argon). In both tests, to vary the constraint around the thermite source, the argon pressure was adjusted up to 1 MPa, and cylindrical devices were settled around the source (see Figure 13).

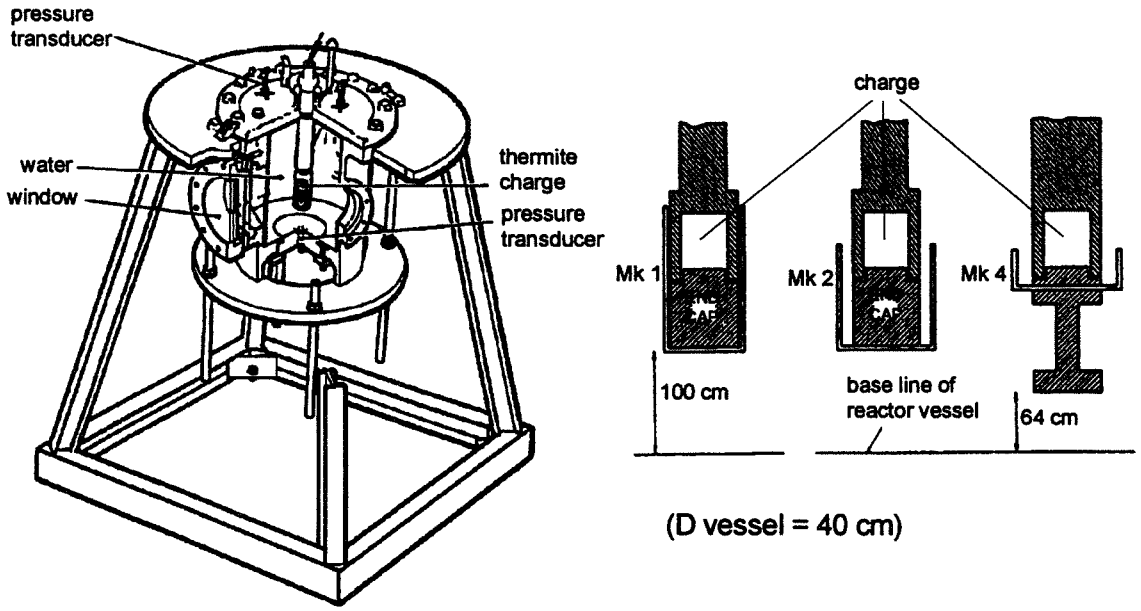

Figure 13 The 0.5-kg thermite experiment and the devices used to increase the constraint around the melt charge.

The experiments were filmed through ports, and pressure was measured both in the water and in the cover gas. The efficiency was deduced from the cover gas compression.

In the small-scale series, 37 tests were carried out without surrounding structures, and the constraints were varied by reducing the initial cover gas volume and increasing the cover gas pressure up to 0.4 MPa. Only 8 SEs were observed, all in experiments with high constraint. The maximum produced energy was 4.19 kJ in test A80, which corresponds to an efficiency of $\eta = 1.8\%$, if we take only the melt that is involved. This melt quantity is estimated from the debris analysis by taking only the debris which have had time to release their heat during the explosion time, which is estimated from the pressure peak rise time. In this case, only the debris with diameters of <150 μm were assumed to be involved. Then, for test A80, only 24% of the melt was involved, which gave an efficiency η_∞ of ~ 0.45, if we take into account all of the melt.

Then 44 experiments were carried out by using the restricted-release devices shown in Figure 13, and 40 SE experiments were observed, which confirmed the importance of the surrounding constraint. Most of them (37 out of 40) were triggered by the impact of the release device on the base of the tank. In these experiments, it was also found that the released energy decreased with water subcooling, whereas the amount of participating melt was almost independent of this subcooling.

At least 11 experiments were carried out in the large-scale facility. They are characterized in Table 1. Except for the fact that multiple interactions were observed, the same tendencies as in the 0.5-kg series were observed:

TABLE 1 Characteristics of SUW Tests[a]

	Initial conditions						Results				
Test	Fuel mass (kg)	Cover gas volume (liters)	Structures	Cover gas pressure (MPa)	ΔT_{sub} (°C)	Goal	Partial H_2 pressure (MPa)	SE number	Mechanical energy (MJ)	Fraction of melt participating (%)	Conversion η ratio (%)
SUW01	24	250	No	0.1	78	Reference	0.23	3	0.223	20.4	2.8
SUW02	24	250	No	0.4	87	Influence of p_∞/SUW01	0.27	0	0.076 (incoherent boiling)	3.9	—
03	24	85	No	0.1	80	Reduction of V_G/SUW01	0.23	2	0.077	12.5	1.6
04	24	250	Yes	0.1	80	Reference influence structure/SUW01	0.23	3	0.175	19.9	2.3
05	24	252	Yes	0.1	61	Influence ΔT_{sub}/SUW04	0.25	2	0.162	13.0	3.2
06	24	271	Yes	0.1	31	Influence ΔT_{sub}/SUW04	0.28	2	0.160	13.1	3.1
07	24	251	Yes	0.1	0	Influence ΔT_{sub}/SUW04	0.42	3	0.225	13.5	4.3
08	24	259	Yes	0.5	60	Influence p_∞/SUW04	0.40	1	0.521	48.2	2.8
09	24	250	Yes	1.0	60		?	1	0.884	75.0	3.0
10	8	250	Yes	0.1	60	Influence M_c	0.18	1	0.118	80.0	1.1
11	8	250	Yes	1.0	60	Influence M_c influence p_∞/SUW10	?	0	0	9.0	—
				(1.0)							

[a]Abbreviations and symbols: P_∞: initial cover gas pressure; M_c: initial melt mass

1. The amount of melt participating in the SE did not depend on the subcooling (SUW 05, 06, 07).
2. The mechanical-energy release increased with ambient pressure (SUW 04, 08, 09).
3. The amount of melt participating in the SE increased with the ambient pressure (SUW 04, 08, 09).

An interesting result was found from this program: The efficiency η calculated by using the amount of participating melt does not depend on the scale, as we can see in Figure 14. The problem is then to be able to estimate this amount of participating melt.

5.3 Conclusions

All of these experimental programs were conducted to produce figures for evaluating the consequences of an SE, that is, to provide information about the efficiency and the amount of participating melt. But to transfer the knowledge obtained from this program by using at most 25 kg of melt to large-scale systems, it appeared that the following approach suffers from simplicity.

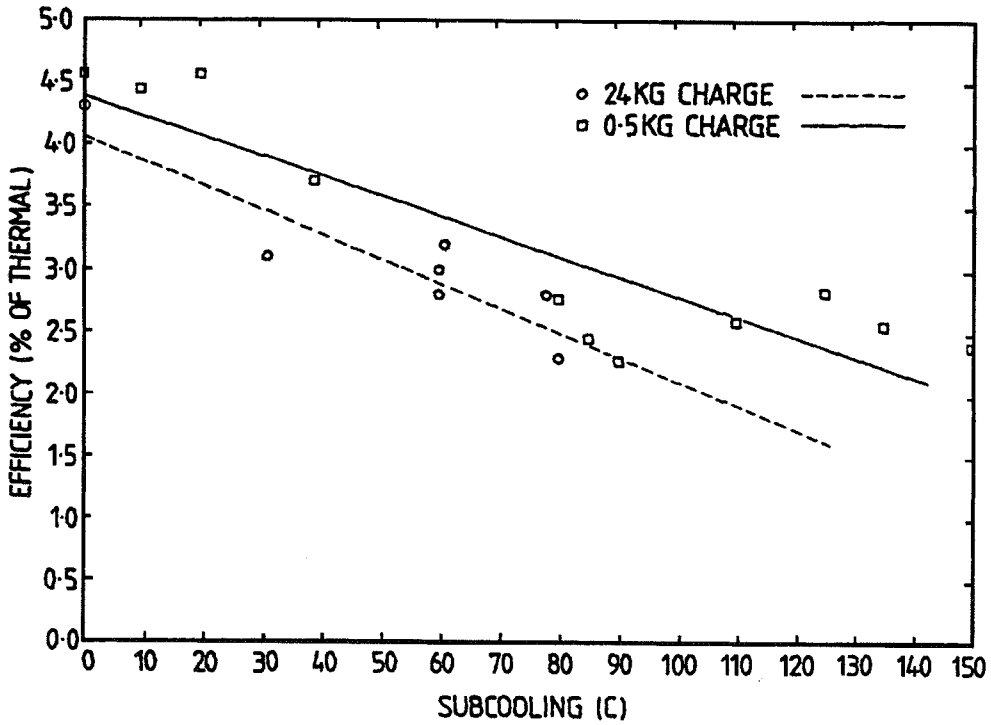

Figure 14 Efficiency η as a function of subcooling in the different Winfrith experiments (0.5–24 kg of melt).

1. Restricting the amount of melt that can participate to an SE may be a trick. In fact, it is likely that all of the melt that flows into the coolant will participate, more or less, in the interaction. If we agree on the usual SE sequence, one triggered somewhere, the SE will propagate through the whole mixture, leading to melt-coolant heat exchanges, more or less efficient depending on the mixture conditions.
2. Using efficiency can also be incorrect for two main reasons. Efficiencies were obtained in rather small-scale experiments (25 kg at maximum) and their transposition to larger scales is difficult for two reasons

   a. We have to take into account the scale effect, which is not firmly established, but there are physical reasons that favor an increase in efficiency with scale. First, as during an SE, heat is transferred from melt to some amount of coolant and then to the surrounding cold coolant; there is a volume-to-surface ratio that characterizes the ratio of the heat received by the coolant (roughly proportional to the volume of the IZ) to the heat lost by the coolant to the surroundings (roughly proportional to the surface of the IZ). So, when the characteristic size L of the IZ increases, this ratio, linked with the SE efficiency, increases proportionally to L. Second, in large-scale systems, the increased constraint allows more time for heat transfer between melt and coolant, which ceases only when the IZ pressure is released (i.e. when the constraint is overcome). We can also expect a higher pressure peak in more constrained systems. However, there is a counter argument; it may be more difficult to have a "good" mixture with a large amount of melt, because more melt implies more vapor production during premixing, that is, less liquid coolant to interact with the melt.
   b. The experimentally deduced efficiency is the response of the experimental loop to the SE, and its use for other conditions with different surroundings has no meaning (see the change between a classical FITS efficiency with a plexiglas wall and the FITS RC2 results). We have to keep in mind that an SE results from the very rapid and intense heat transfer between melt and coolant caused by fine and efficient FR. Then, the heated and pressurized coolant expands against the surroundings, and it is during this expansion phase that most of the mechanical energy is released. There is then a constraint effect.

For these reasons, from 1985, the approach for estimating the risks induced by large SEs has changed and tended to be more rational. Advances in computer systems and in physical knowledge allow people to build multidimensional and multifield computer codes dealing with all the phases of an SE.

6. PRESENT APPROACH IN THE TREATMENT OF A STEAM EXPLOSION

The first integrated code dealing with all the phases of an SE was developed at Sandia National Laboratory by Young (44); it is the Integrated Fuel Coolant Interaction (IFCI) code. The idea was then used by Medhekar et al (University of California Santa Barbara) (45), who extended the possibility of their premixing code (PM alpha) and built the ESPROSE code to deal with the propagation phase of an SE, while the MC3D code (46) and IVA3 code (47) started to be developed in three-dimensional geometry. Now other integrated codes are being developed and validated, like COMETA (48) and JASMINE (49).

Such codes are built to follow the physics of an SE and will evolve to include the more recent knowledge concerning the physics of SEs. When these codes are sufficiently validated (and they are close to being so), they will provide tools for extrapolating from small- and medium-scale experiments to larger systems, taking into account properly the scale and constraint effects. By sufficiently validated, we mean that " . . . one would be able to demonstrate 'fitness for purpose' by ensuring that data are available to support the constitutive physics in key areas of parameter space relevant to large-scale predictions, and to demonstrate broad consistency with the results of test series" (50).

These key physics for the different phases of an SE are now presented together with the experimental programs built for validation.

6.1 Premixing

It has long being recognized that premixing is necessary for SEs involving tons of melt. This was roughly demonstrated by Cho et al (51) in 1976. They considered the energy required to fragment and mix a volume V_c of fuel into fragments of size R_c based on the scheme illustrated in Figure 15.

They evaluated

1. The energy E_s required to create the surface of particles, such that

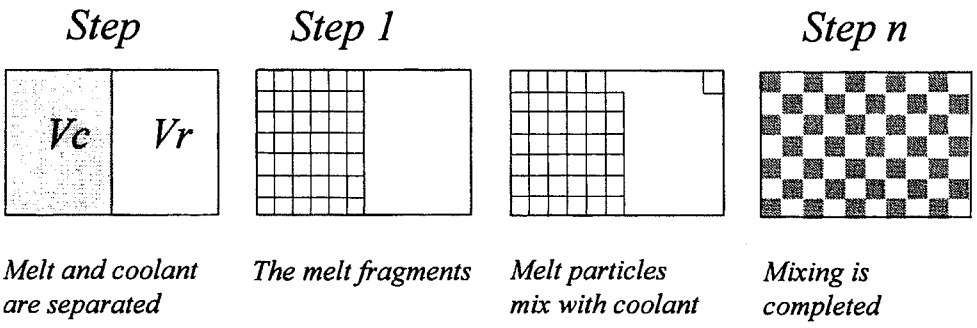

Figure 15 Steps in premixing in the Cho et al approach (51).

$$E_s = \text{number of particles} \times \text{surface energy of a particle}$$
$$= (3V_c/R_c)\sigma_c;$$

2. the kinetic energy required to displace the particles, shown as

$$E_c = \text{number of particles} \times \text{kinetic energy of a particle}$$
$$= N_p \cdot \frac{4}{3}\pi\rho_c R_c^3 \cdot \frac{U_p^2}{2},$$

with

$$U_p = \frac{\text{characteristic length of the mixing domain}}{\text{characteristic time for fragmentation and mixing}}$$
$$= \frac{L_M}{t_m} \approx \frac{V_c^{1/3}}{t_m};$$

3. the energy required to overcome the drag during particle displacement, shown as

$$E_f = \text{number of particles} \times \text{drag work during particle displacement},$$
$$E_f = N_p \cdot C_D \cdot \frac{1}{2}\rho_r U_p^2 \pi R_c^2 \cdot L_M \approx V_c\left(\frac{3}{8}\rho_r U_p^2\right)\frac{L_M}{R_c} \quad (C_D \approx 1).$$

Then Cho et al (51) showed that it is impossible to get an SE in a single step, that is, by going from step 0 to the final step ($R_c = \sim 100$ μm) in a time characteristic of an SE, that is, $t_m = \sim 1$ ms because the energy to fragment and mix is larger than the thermal energy of the melt. But if we have a premixing phase in which 1-cm fragments are produced in a second time scale, followed by an explosion phase in which 100-μm fragments are produced in a millisecond time scale, the FR-mixing energies are far smaller than the thermal one.

The knowledge of premixing is important because it gives information about the initial conditions for the explosion, which are important in the assessment of the consequences. The most important quantity to evaluate is the amount of steam produced, which limits the interfacial area between melt and coolant that is the most important quantity in the calculation of the explosion. Some authors, like Henry & Fauske (52), thought of finding some limits to mixing based on the idea of the fluidization of the melt by the steam produced. However, their hypotheses were too crude, and improvements of their analysis showed that this limit to mixing was difficult to assess. Nevertheless, they were the first to stress the importance of the water depletion effect. Another important quantity to evaluate is the melt length scale, which influences the vapor production during premixing and the fine FR kinetics responsible for the explosion (superficial solidification of the melt may even suppress the fine FR). Some people even thought that the use of a predispersed melt may suppress the explosion. For example, in the alpha

facility at Japan Atomic Energy Research Institute (53), they dropped 20 kg of an iron-alumina melt (like in FITS) into water and sometimes used a dispersion device made of 2-mm-diameter steel wire on a 25-mm grid to prefragment the melt stream before its contact with water, thereby enhancing the mixture void fraction. The JAERI workers effectively concluded that the dispersion device enhances steam generation, but does not necessarily result in the suppression of spontaneous SEs. They even got one of their most energetic SEs with an average void fraction of 0.63 in test STX021.

The description of premixing obviously depends on the way melt and coolant are brought into contact. As we already said, there are three main modes of contact: (*a*) the melt can be poured into the coolant, which is the most common situation; (*b*) the coolant can be injected into the melt, which is very difficult owing to thermal and density effects (melt is usually denser than coolant); and (*c*) melt and coolant can be in a stratified geometry.

Here we concentrate on the most common contact mode, pouring of the melt into the coolant. In this case, the key physics to assess are (*a*) the FR of the hot-melt jet during its penetration into the coolant, (*b*) the fragmentation of the droplets (issued from the melt) into the two-phase coolant, (*c*) the vapor production by the hot melt, and (*d*) the dispersion of the melt droplets by the two-phase coolant flow.

6.1.1 Melt Jet Fragmentation If jet FR has received a lot of attention in isothermal conditions, there are few studies devoted to the FR of a hot-melt jet into water under boiling conditions. For isothermal jets, depending on the jet Reynolds number ($Re_j = \rho_j D_j V_j/\mu_j$) or the jet Weber number ($We_j = \rho_j V_j^2 D_j/\sigma_j$), the jet may fragment by a number of mechanisms, as shown in Figure 16. As the jet Reynolds number increases, we have successively, (*a*) the Rayleigh regime governed by surface tension, (*b*) the transition regime in which the inertial forces of the surrounding medium accelerate the breakup process into drops on the order of the jet diameter (large-scale instability), and (*c*) the turbulent regime in which drops much smaller than the jet diameter are formed by small-scale instabilities, which are dependent on ambient conditions. At the head of the jet, we may also have a ball caused by the resistance of the ambient fluid; but if the jet reaches a steady state where it is fully fragmented, this head should disappear.

For a hot-melt jet into water, steam is produced as soon as the melt contacts the water. If water is subcooled, this may have only a minor effect, but if water is close to saturation, it will have a big effect. This was recognized by Epstein & Fauske (54), who provided the first model describing the jet fragmentation by the stripping of Kelvin Helmholtz instabilities along the tail of the jet (see in Figure 16c), using for the properties of the ambient medium those of water for thin film (subcooled water) or those of steam for thick film (almost saturated water).

This type of modeling, based on the growth of small-scale instabilities along the jet tail, which is now recognized as the dominant FR mechanism, was then improved in (*a*) the THIRMAL code in ANL (55), (*b*) the IKEJET code at Stutt-

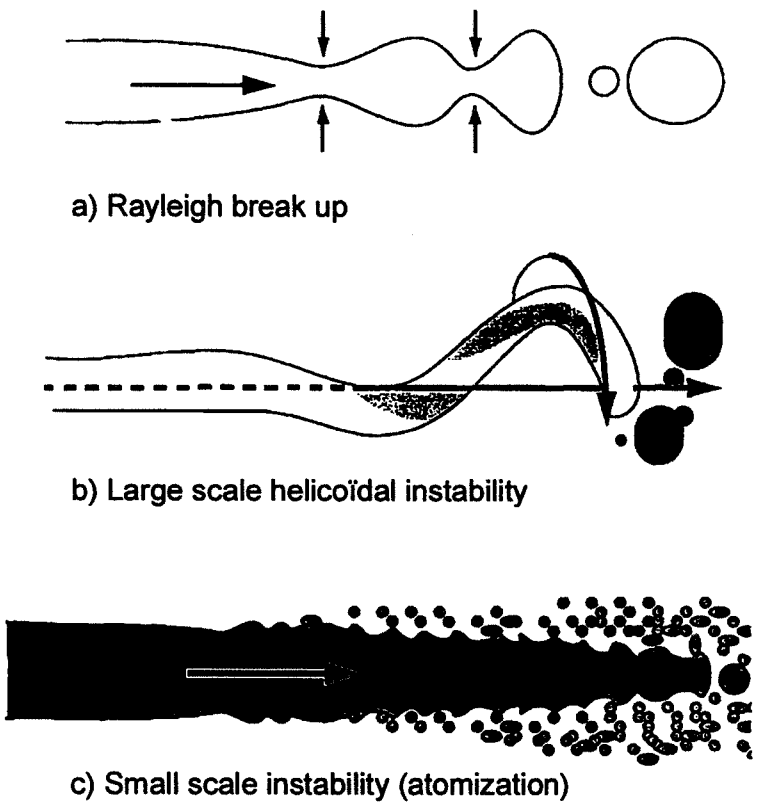

Figure 16 Jet fragmentation mechanisms.

gart University (56), which allows a shear layer profile around the jet (Jeffrey-Miles formulation) rather than a tangential discontinuity, and (*c*) the COSTA model at CEA-Grenoble (57), which extended the Jeffrey-Miles approach to include the variation of steam properties (density and viscosity) caused by the high temperatures gradient in the steam film. The few relevant experiments used for model validation are briefly described in the above references.

6.1.2 Drop Fragmentation The drops issued from the jet can again be fragmented by the two-phase coolant flow. Hydrodynamic FR by the relative flow is again assumed to be the dominant mechanism and, again, most of the data and models come from isothermal experiments. A key paper is by Pilch & Erdman (58), in which isothermal liquid-gas and liquid-liquid hydrodynamic FR of drops is analyzed by using the Weber number $We = \rho_c V_{rel}^2 D/\sigma$, where ρ_c = density of the continuous fluid and V_{rel} = relative velocity, and in which the FR characteristic time, as well as the size of the fragments, is given. However, for premixing calculations, we have a two-phase coolant, and the difficulty is to transfer Pilch results, for example, to three-phase flow (the presence of other melt droplets may even influence the density of the surrounding medium).

6.1.3 Vapor Production When the melt droplets first contact the coolant, their temperature is such that stable film boiling occurs. Film boiling of spheres at high

temperature (2000°C) in single- and two-phase coolant film has been assessed only recently by Liu & Theofanous (59). Description of radiative heat transfer is also important, particularly the evaluation of the part of this radiative flux that is absorbed in the vicinity of the vapor-liquid interface and that produces vapor. Owing to the high temperature of the melt, vapor is heated within the film, and a description of the recondensation is also of importance. The three-phase aspect of the mixture is also difficult to describe precisely.

6.1.4 Dispersion of the Melt in the Two-Phase Coolant Again, it is the three-phase aspect that is difficult to handle. In fact, drag coefficients for droplets and bubbles flowing in a single fluid have been established by Ishii & Mishima (60) for 1D flow. Owing to the transient aspect of the process, the large density differences, and the volumetric concentration gradients, other terms may be necessary, like virtual mass, lift, and turbulent dispersion (61).

Specific experiments have been performed to validate both heat transfer and dispersion by using solid spheres at high temperature (≤2000°C–2500°C) dropped into subcooled and saturated water. These are the MAGICO (62), BILLEAU (63), and QUEOS (64) tests. To validate the premixing code, an experiment with ~150 kg of a UO_2-ZrO_2 mixture at ~3000°C has been built in ISPRA: the FARO experiment (65). In this experiment a jet of corium (D_j = 10 or 5 cm) is dropped into water, so that all of the physics of premixing are involved, and it is possible to validate globally the premixing codes through the available results—pressure increase in the vessel caused by the steam production and overall energy balances through temperature measurements in the fluid and in the walls.

6.2 Triggering

The trigger is the event that induces a transition between the premixing sequence and the propagating phase by locally initiating a rapid heat transfer and pressure rise that will eventually escalate during its propagation within the mixture. It is now accepted that the trigger results from the collapse of the insulating, vapor film around the melt droplet. This collapse may be a result of the melt cooling (the surface temperature falls below the minimum film boiling temperature) or may be induced by an external event leading to a pressure pulse. This external event may result from contact of the melt with structures, entrapment of some coolant within the melt during its fall or between the melt and a structure, the restart of a pump, and so forth.

High-speed movies (10^4 to 10^5 pps) show (26, 67) that film collapse is rapidly followed by local eruptions from the fuel surface. However, the mechanisms leading to these eruptions are not yet clear. For some authors, they are associated with the vaporization of coolant jets produced by Rayleigh-Taylor instabilities at the vapor-liquid interface. There jets can either penetrate the fuel and then vaporize suddenly when reaching the superheat limit (65, 68), or produce "splashes" when contacting the melt surface, as proposed by Ochiai & Bankoff (69). Another

possible mechanism can be the "drop capture model" of Henry et al (40), who showed that, if the instantaneous contact temperature is greater than the spontaneous nucleation temperature of the coolant, under certain conditions the liquid coolant may wet and be captured by the hot liquid surface and, so, could vaporize suddenly.

Many other mechanisms have been postulated. In his review, Corradini et al (7) found >40 of them. Some of them have hydrodynamic causes, others are linked with thermomechanical stresses appearing in the solidifying external shell, and so forth.

The effects of parameters like coolant subcooling, ambient pressure, presence of noncondensable gases (owing to chemical reaction for example), and solidification have already been addressed in the analysis of small-scale FCI experiments.

6.3 Propagation

Once triggered, the explosion will propagate and may escalate through the premixture. The pressurization induced by the trigger will destabilize the surrounding vapor films, inducing more fine FR, so more vaporization and the process may result in an escalation.

The key physics to assess this are then (*a*) the identity and kinetics of FR mechanisms during the escalation and propagation phase, and (*b*) how heat is transferred from the fragmented debris to the liquid coolant into which they are ejected.

6.3.1 Fine Fragmentation It is generally accepted that, during the escalation, the FR mechanism changes from a "thermal" one (similar to the one involved in the triggering), during the early phase of the escalation when the pressure rise is not too high, to a hydrodynamic one owing to the velocity difference between melt and coolant induced by high-pressure propagation. Because thermal-FR processes have already been discussed (cf triggering), only the hydrodynamic FR will be presented. Once again, these processes have been widely studied in isothermal conditions [see Pilch & Erdman (58) or Tan & Bankoff (70)], but no final conclusions have yet been drawn. There is still a debate about the dominant hydrodynamic fragmentation mechanism, which might include (*a*) stripping of fine droplets by boundary layer effects and surface instabilities (Kelvin-Helmholtz type) as favored by Burger et al (71) in their 1D propagation code FRADEMO; (*b*) Rayleigh-Taylor instabilities on the windward side of the melt drops owing to the acceleration by the ambient coolant flow (if the melt has a higher density than the surrounding coolant) as used by Chen et al (72); or (*c*) a combination of both as found by Baines (73), who found that boundary-layer stripping is dominant for $200 \leq We \leq 2000$ ("liquid filaments are stripped from the equator"), whereas for a higher Weber number, " . . . there is also evidence of RT instabilities on the front face of the drop." For Kelvin-Helmholtz instabilities, the governing

dimensionless number is the Weber number We $= \rho_c V_{\text{rel}}^2 D/\sigma$, whereas for Rayleigh-Taylor instabilities, it is the Bond number Bo $= \rho_d a D^2/\sigma$. But for spherical droplets, we can estimate the acceleration by using the classical drag law, that is

$$\rho_d \frac{\pi D^3}{6} a = C_D \frac{1}{2} \rho_c V_{\text{rel}}^2 \frac{\pi D^2}{4},$$

where D is the dispersed phase. So we get Bo $= (6/8) C_D$ We, where C_D is ~2.5 for the fragmenting drop (58). That means, because the two governing dimensionless numbers are proportional, that we are not able to choose the FR mechanism from an analysis of experimental breakup time.

For boundary layer stripping, it is usually found that the dimensionless FR time, defined by $t^* = t[(V_{\text{rel},0}/D_0)(\sqrt{\rho_c/\rho_d})]$, is constant at ~4, when initial values are used, or around 1.25 if we use instantaneous values for V_{rel} and D (74), while for RT instabilities, it is related to the Bond number through a relation like:

$$t_{fr}^* \approx 10.3 \text{ Bo}_o^{-1/4}$$

or $t_{\text{fr}}^* \approx 14.8 \text{ Bo}_i^{-1/4}$ (75–76), where i is instantaneous.

In the propagation codes, the hydrodynamic FR rate is often described by assuming $(dm_{\text{fr}}/dt) \approx (m_0/t_{\text{fr}}^*) \approx (m_i/t_{\text{fr},i}^*)$ (i.e. linearizing the FR process and heuristically extending it to instantaneous values). By doing so, FR correlations can be derived as

$$dm_{fr}/dt = C_{fr} \times V_{\text{rel}}(t)\pi D^2(t)(\rho_c \rho_d)^{1/2}$$

for boundary layer stripping (C_{fr} = constant), or

$$dm_{fr}/dt = [1/6t_{fr}^*(t)]\ [V_{\text{rel}}(t)\pi D^2(t)(\rho_c \rho_d)^{1/2}]$$

with $t_{\text{fr}}^* = \beta_{\text{fr}} \text{ Bo}_i^{-1/4}$ for IRT with β_{fr} = constant to be deduced from experiments.

To solve this fine-FR issue, two facilities have been built: (*a*) the SIGMA facility (76–77), in which high-temperature melt drops (tin, gallium, and steel at temperatures ≤2000 K) are submitted to shock waves of ≤27.2 MPa in a shock tube geometry; and (*b*) the DROPS facility (78), in which high-temperature melt drops (gallium, woods metal, and tin at temperatures ≤1300 K) are submitted to a coolant flow produced by a piston. In addition to high-speed photography, the SIGMA facility has the advantage of using flash X-rays to evaluate the amount of fragments versus time.

It must also be mentioned that, in some experiments with woods metal, or mercury drops falling into a glycerin/water mixture, Bankoff and coworkers (72–81) found that the drop first deformed into a spherical cap drop with an irregular rear surface and then began to swell up, indicating entrapment of the glycerin/water mixture into the drop. It has been suggested that it is the vorticity generated at the sharp trailing edge of the drop that is responsible for this entrapment. In

that case, this FR could be called a "thermal" one, driven by hydrodynamic effects (like coolant jet impingement induced by film boiling destabilization).

6.3.2 Heat Transfer Between Melt Debris and Coolant To get a rapid escalation after triggering, high heat transfer rates are necessary. Some are produced by the increase in interfacial area caused by fine FR of the melt drops, but, owing to the ongoing production of new melt-coolant contacts, it is also expected that, transiently, a high heat transfer coefficient can be obtained. Because of this transient aspect, it has long been suspected (80–82) that the coolant temperature in the interaction zone may not be uniform, as it was postulated in the first detonation models. This has led to two different modeling approaches. (*a*) In the microinteraction concept proposed by Chen et al (72) and Yuen & Theofanous (83), heat from the fuel debris is transferred to only part of the liquid coolant. This heated part varies with time and is determined by considering the entrainment of cold coolant into the microinteraction field (debris + coolant assumed in thermal equilibrium) during melt FR. In that case, the pressure buildup is linked to the thermal expansion of the hot liquid coolant. (*b*) In the nonequilibrium steam production proposed by Berthoud & Brayer (84) and also used by Corradini & Tang in their 1D code Texas (85), part of the heat from the fuel debris is used to produce vapor at the vapor liquid interface under thermal nonequilibrium. In that case, the pressure buildup is linked to phase change.

These two concepts are presented in Figure 17. In the nonequilibrium approach, the heat transfer coefficients between melt debris and interface and between interface and bulk coolant should be provided. They are deduced from experiments in which the transient quenching of a hot material is investigated. They are of three types: (*a*) those in which the collapse of a vapor film by a pressure pulse is studied (86); (*b*) those in which a wire or a foil originally

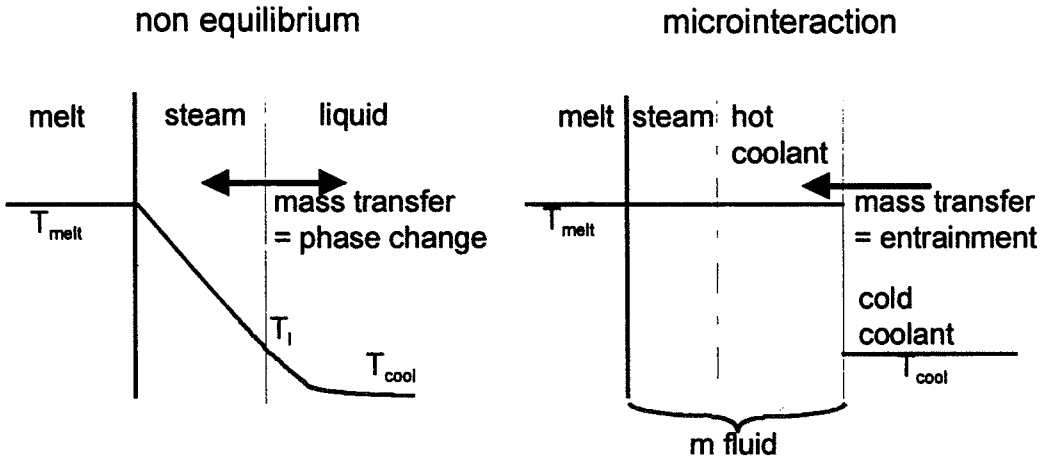

Figure 17 Temperature profiles in the interaction zone in the nonequilibrium and the microinteraction modeling approaches to melt-coolant contacts.

immersed in the coolant is subject to a heat pulse (87); and (*c*) those in which an initially heated wire is quenched in a coolant (88).

All of these experiments concluded that heat transfer coefficients as high as 10^5 W m^{-2} K^{-1} can be obtained during the transient quenching of the debris. On the coolant side, heat transfer can be evaluated by using a transient-conduction approach or an increased-convection coefficient to take into account the unstable behavior of the interface as observed in the EXCOBULLE experiment (89). In this experiment, entrainment of cold water into the hot expanding vapor was characterized, similarly to the entrainment concept in the microinteraction approach but on a larger scale. The nonequilibrium approach is extended to supercritical conditions; as around the melt debris, there will always be a hot phase (pseudosteam) surrounded by a colder one (pseudoliquid) separated by a pseudointerface assumed at the pseudocritical temperature that corresponds to the peak value of the heat capacity, as shown on Figure 18. The two approaches are presented and discussed elsewhere (90).

Finally, to validate the propagation phase models of an SE, almost 1D shock tube experiments have been developed. In these experiments, kilograms of high-temperature melt are dropped into a vertical tube filled with water. The first one was performed by Baines (82) and used 1.5 kg of tin at 800°C. Peak pressures on the order of 4–10 MPa were reached, and propagation velocities from 50 to 250 m/s were measured. Baines also pointed out in his analysis that most of the water remains unheated during propagation and that only a thermal boundary layer of 10–100 μm was involved during the transient heat transfer. Later, the same type of apparatus was used by Park et al (91).

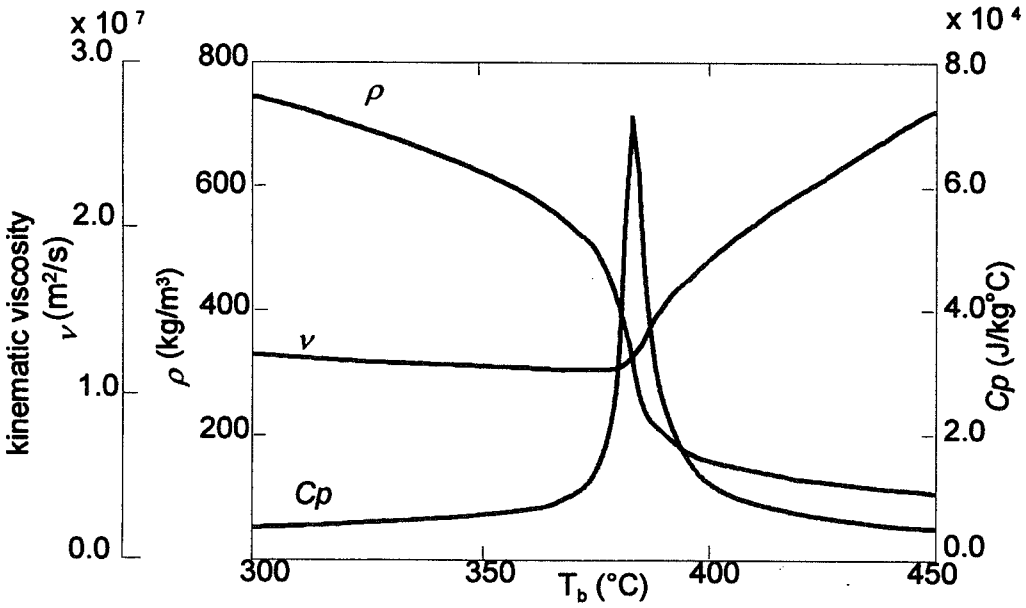

Figure 18 Physical properties of supercritical water near the pseudocritical temperature $T = 383$°C at $P = 2.452 \times 10^7$ Pa.

Finally, in the KROTOS tests in JRC Ispra (92), kilograms of tin, Al_2O_3, or UO_2-ZrO_2 mixture are also dropped into water. Explosions can be triggered or spontaneous. It has been found that tin and Al_2O_3 melts explode easily, whereas it is very difficult to trigger a UO_2-ZrO_2 melt. Only very small propagating events have been obtained when the ambient pressure is raised to 0.36 MPa (the loop limit) to reduce the volumetric amount of steam during premixing. There are many reasons for this nonexplosivity. Two of these include the following:

1. During premixing, UO_2-ZrO_2 is much more fragmented than Al_2O_3 (1 order of magnitude smaller, but this cannot yet be modeled), so more vapor is produced, and external solidification of the melt is easier.
2. It has been found that hydrogen is produced when UO_2-ZrO_2 contacts water (the cause and kinetics are still not clear), and it is known that noncondensable gases do not help to produce a SE (triggering is more difficult).

We must also say that it is not very easy to validate propagation codes with these experiments as the initial conditions at triggering; that is, the result of premixing are not measured precisely, and it is known that premixing conditions have a large influence on the explosion behavior.

7. CONCLUSIONS

The present knowledge and predictive capabilities about the SE problem have been briefly presented. It is thought that scale and constraint effects can be assessed only through the use of sufficiently validated codes. These codes are in the validation process, but open questions still remain regarding (*a*) the melt jet fragmentation, (*b*) the general problem of extending two-phase constitutive laws to multiphase systems, (*c*) the triggering mechanisms, (*d*) the nonequilibrium aspect for the coolant in the interaction zone, and (*e*) the effect of noncondensable gases, of additional chemical reactions that may increase the delivered energy, of solidification, of ambient pressure, and so forth, on the explosivity of a melt-coolant mixture. In addition, there are other modes of contact, like coolant injection into melt and stratified geometry. More detailed review papers can add to this presentation. Some of them have already been quoted (7, 20, 22), and we add others here (93–95).

LITERATURE CITED

1. Cronenberg AW, Benz R. 1978. Vapor Explosion Phenomena with Respect to Nuclear Reactor Safety Assessment, US Nuclear Regulatory Commission/ CR.O245-TREE-1242
2. 1976. The explosion at the Appleby-Frodingham steelworks, Scunthorpe, 4 November 1975. In *Health and Safety Executive Report.* London: HMSO
3. Katz DL, Sliepcevich CM. 1971. LNG/ water explosions: cause and effect. *Hydrocarb. Process.* 50:240–44
4. Fujii N. 1995. Various styles of intense multiphase interactions viewed from volcanic explosions. *Proc. US (Natl. Sci. Found.-Japan (Jpn. Soc. Promo. Sci.) Joint Semin.—June 9–13, 1995.* Santa Barbara, Calif.
5. Buxton LD, Nelson LS. 1974. Steam Explosions, *Rep., SAND 74-0382-Chapter 6,* Sandia Natl. Lab., Albuquerque, NM
6. Hicks EP, Menzies DC. 1965. Theoretical studies on the fast reactor maximum accident. *Proc. Conf. Saf., Fuels Core Des. Large Fast Power React.-Argonne National Laboratory-7120.*
7. Corradini ML, Kim BJ, Oh MD. 1988. Vapor explosions in LWR: a review of theory and modeling. *Prog. Nucl. Energy* 22(1):1–117
8. Cronenberg AW, Grolmes MA. 1975. Fragmentation modeling relative to the breakup of molten UO_2 in sodium. *Nucl. Saf.* 16:683–700
9. Briggs AJ. 1976. Experimental studies of thermal interactions at AEE Winfrith. *Proc. Comm. Saf. Nucl. Install. Meet. Sodium-Fuel Interact. Fast React., Tokyo,* pp. 75–96
10. Board SJ, Hall RW. 1976. Recent advances in understanding large scale vapor explosions. *Proc. Comm. Saf. Nucl. Install. Meet. Sodium-Fuel Interact.* Fast Reactor, Tokyo, pp. 249–93
11. Board SJ, Hall RW, Hall RS. 1975. Detonation of a fuel coolant explosion. *Nature* 254:319–321
12. Katz DL. 1972. Superheat limit explosions. *Chem. Eng. Prog.* 58:(5); 68–69
13. El Genk MS. 1981. MFCI Occurring During a Severe Reactivity Initiated Accident Experiment, *Rep. NUREG/CR. 1900, EGG-2080.* Idaho Natl. Lab., EGG Idaho, Inc. Idaho Falls, ID
14. Zeldovich IB, Kompaneets AS. 1960. *Theory of Detonation.* London: Academic
15. Scott E, Berthoud G. 1978. Multiphase thermal detonation. In *Topics in Two Phase Heat Transfer and Flow,* ed. SG Bankoff, pp. 11–16. New York: Am. Soc. Mech. Eng.
16. Berthoud G, Scott E. 1979. Multiphase thermal detonation for a UO_2-N_a system *Proc. Comm. Saf. Nucl. Install. Spec. Meet. FCI Nucl. React. Saf., 4th, Bournemouth, UK,* UKAEA-AEE Winfrith pp. 22–53.
17. Goldhammer H, Mehr K, Kottowski HM. 1982. Influence of non-uniform temperature distribution on the C–J condition in UO_2/N_a thermal detonation. OECD-FCI Newslett. No. 2, SINDOC (82)1, CSNI-OECD. Nucl. Energy Agency, Paris
18. Sharon A, Bankoff SG. 1978. Propagation of shock waves in a fuel-coolant mixture. In *Topics in Two Phase Heat Transfer and Flow,* ed. SG Bankoff, pp. 51–77. New York: Am. Soc. Mech. Eng.
19. Cho DH, Ivins RO, Wright RW. 1971. Pressure generation by molten FCI under LMFBR accidents conditions. Presented at Am. Nucl. Soc. Top. Meet. New Dev. React. Math. App. Idaho Falls, ID
19. (a) Berthoud G, Newman W. 1984. A description of a fuel-coolant thermal interaction model with application in the

interpretation of experimental results. *Nucl. Eng. Des.* 82:381–91
20. Berthoud G. 1987. L'interaction corium-eau: synthèse et analyse des résultats expérimentaux, *Note STT/LPML/87/28C,* Commis. Energ. At., Grenoble, France
21. Fletcher DF. 1995. Steam explosion triggering: a review of theoretical and experimental investigations. *Nucl. Eng. Des.* 155:27–36
22. Buxton D, Nelson LS, Benedick WB. 1979. Steam Explosion Triggering and Efficiency Studies, *Rep. SAND-79-0261 C.* Sandia Natl. Lab., Albuquerque, NM
23. Corradini ML. 1980. Analysis and modeling of steam explosion experiments, *NUREG/CR-2072, SAND 80-2131, R3,* Sandia Natl. Lab., Albuquerque, NM
24. Nelson LS. 1980. Steam explosions in the molten iron oxide/liquid water system. *High Temp. Sci.* 13:235–56
25. Mitchell DE, Corradini ML. 1981. Intermediate scale steam explosion phenomena: experiments and analysis, *NUREG/CR-2145, SAND 81-0124, R3,* Sandia Natl. Lab., Albuquerque, NM
26. Nelson LS, Duda PM. 1981. Steam explosion experiments with single drops of iron oxide melted with a CO_2 laser, *NUREG/CR-2295, SAND 81-1346 R3,* Sandia Natl. Lab., Albuquerque, NM
27. Mitchell DE, Evans NA. 1982. Effect of water and fuel masses on the behavior of molten core-coolant interactions at intermediate scale, *SAND-82-0407 C,* Sandia Natl. Lab., Albuquerque, NM
28. Nelson LS, Duda PM. 1985. Steam explosion experiments with single drops of iron oxide melted with a CO_2 laser. Part II. Parametric studies, *NUREG/CR-2718, SAND 82-1105, R3,* Sandia Natl. Lab., Albuquerque, NM
29. Evans NA, Mitchell DE, Nelson LS. 1982. Recent results from the Sandia Steam Explosion Program, *SAND 82-2269 C,* Sandia Natl. Lab., Albuquerque, NM
30. Berman M, McGlaun JM, Corradini ML. 1983. Core melt/coolant interactions: modelling, *SAND 83-1852 C,* Sandia Natl. Lab., Albuquerque, NM
31. Berman M, Swenson DV, Wickett AJ. 1984. An uncertainty study of P.W.R. steam explosions, *NUREG/CR-3369, SAND 83-1438, R1,* Sandia Natl. Lab., Albuquerque, NM
32. Mitchell DE, Evans NA. 1986. Steam explosion experiments at intermediate scale: FITS B Series, *NUREG/CR-3983, SAND 83-1057, R3,* Sandia Natl. Lab., Albuquerque, NM
33. Berman M. 1986. LWR Safety Research Program. Semiannual Report—Oct.83–March 84', *NUREG/CR-4459, SAND 85-2500, R3,* Sandia Natl. Lab. Albuquerque, NM
34. Nelson LS, Duda PM. 1982. Steam explosion of a metallic melt as its degree of oxidation increases: Fe, $FeO_{1,O}$ and $FeO_{1,2}$, *CONF 820802—17, SAND-820441 C,* Sandia Natl. Lab., Albuquerque, NM
34. (a) Cole RH. 1948. *Underwater Explosions.* Princeton, NJ: Princeton Univ. Press
35. Henry RE. 1995. Externally triggered steam explosion experiments: amplification or propagation. *Nucl. Eng. Des.* 155:37–44
36. Okkonen T, Okkanen T, Seghal BR. 1997. Experiments on melt drops falling into a water pool. *Proc. Org. Econ. Coop. Dev./Comm. Saf. Nucl. Install. Spec. Meet. FCI, Tokai-mura, Japan,* pp. 658–73
37. Dullforce TA, Buchanan DJ, Peckover RS. 1976. Self-triggering of small scale FCI. I. Experiments. *J. Phys. D. App. Phys.* 9:1295–1303
39. Fauske HK. 1974. Some aspects of liquid heat transfer and explosive boiling. Presented at Fast React. Saf. Meet., Beverly Hills
40. Henry RE, Fauske HK. 1976. Nucleation characteristics in practical explosions. Presented at Spec. Meet. Sodium-Fuel Interact. Fast React., *3rd,* Tokyo
41. Bird MJ, Millington RA. 1979. FCI studies with water and thermite generated molten uranium dioxide. Presented at Comm.

Saf. Nucl. Install. Spec. Meet. FCI Nucl. React. Saf., 4th, Bournemouth, UK
42. Bird MJ. 1981. *Thermal interactions between molten uranium dioxide and water: an experimental study using thermite generated uranium dioxide.* Presented at Winter Ann. Meet. Am. Soc. Mech. Eng., Washington, DC
43. Bird MJ. 1984. An experimental study of scaling in core melt/water interaction, *PWR/SAWG/P (84) 71.* Presented at Natl. Heat Transfer Conf., 22nd, Niagara Falls
44. Young MF. 1987. An integrated code for calculations of all phases of FCI—*NUREG/CR-5084-SAND 87-1048.* Sandia Natl. Lab., Albuquerque, NM
45. Medhekar S, Amarasooriya WN, Theofanous TG. 1989. Integrated analysis of steam explosion. *Proc. Int. Top. Meet. Nucl. Therm. Hydraul., 4th, Karlsruhe,* ed. U Müllerelal. F2K Karlsruhe. F.R.G.
46. Berthoud G, Valette M. 1993. Calculations of the premixing phase of a FCI with the MC3D code. Presented at Comm. Saf. Nucl. Install. CSNI Spec. Meet., Santa Barbara
47. Jacobs H. 1993. *Analysis of large scale melt water mixing events.* Presented at Comm. Saf. Nucl. Install. Spec. Meet., Santa Barbara
48. Annunziato A, Yerkess A, Addabbo C. 1997. FARO and KROTOS code simulation and analysis at JRC ISPRA. *Proc. Comm. Saf. Nucl. Install. Spec. Meet. FCI, Tokai-mura, Japan,* pp. 751–68
49. Yang Y, Moriyama K, Maruyama Y, Park HS, Sugimoto J. 1998. Five component propagation model for SE Analysis. Presented at Severe Accid. Res. Japan Meet., Tokyo
50. Turland BD, Dobson GP, Birchley JC. 1996. State of the Art Report on Molten Fuel Coolant Interactions, *Rep. EUR 16874 EN,* European Commission, Brussels
51. Cho DH, Fauske HK, Grolmes M. 1976. Some aspects of mixing in large mass energetic FCI. *Proc. Int. Meet. Fast React. Saf. Rel. Phys., Vol. 4, Chicago,* pp. 1852–61. CONF.761009, Natl. Tech. Info. Serv. US Dep. Commerce
52. Henry RE, Fauske HK. 1981. Required initial conditions for energetic steam explosion, *ASME.HTD.V19,* Am. Soc. Mech. Eng., Washington, DC presented at the Winter Annual Meeting of Am. Soc. Mech. Eng., Washington DC, Nov. 15–20 ed. ML Corradini (U. Wisconsin. Madison), AA Bishop (U. Pittsburgh), Am. Soc. Mech. Eng. N.Y., pp. 99–108
53. Yamano N, Moriyama K, Maruyama Y, Kudo T, Sugimoto S. 1995. Study of premixing phase of a steam explosion in ALPHA program. *Proc. US Natl. Sci. Found.-Japan (JSPS) Joint Semin., Santa Barbara,* pp. 81–97
54. Epstein M, Fauske HK. 1985. Steam film instability and the mixing of core melt jets and water, Presented at Am. Soc. Mech. Eng./AICE Natl. Heat Transf. Conf., Denver
55. Chu C, Sienicki JJ, Spencer BW, Frid W, Löwenhielm G. 1995. Ex Vessel melt coolant interactions in deep water pool: studies and accident management for Swedish BWRS, *Nucl. Eng. Des.* 155:159–213
56. Burger M, Cho SH, Berg EV, Schatz A. 1995. Breakup of melt jets as precondition for premixing: modeling and experimental verification. *Nucl. Eng. Des.* 155:215–51
57. Meignen R, Berthoud G. 1997. Fragmentation of molten fuel jets. *Proc. Int. Semin. Vapor Explosions Explosive Eruptions, Sendai, Japan* 83–100
58. Pilch M, Erdman CA. 1987. Use of breakup time data and velocity history data to predict the maximum size of stable fragments for acceleration induced breakup of a liquid drop. *Int. J. Multiphase Flow* 13(6) 741–57
59. Liu C, Theofanous TG. 1994. Film boiling on spheres in single and two phase flows, *DOE/ER/12933 Fin. Rep.* US Dept. Energy, Washington, DC
60. Ishii M, Mishima K. 1984. Two fluid model and hydrodynamic constitutive relations. *Nucl. Eng. Des.* 82:107–26
61. Lahey RT, Lopez DE, Bertodano M. 1991. The prediction of phase distribu-

tion using two fluid models. *Proc. Am. Soc. Mech. Eng./Jpn. Soc. Mech. Eng. Therm. Eng., Vol. 2,* pp. 193–200
62. Angelini S, Theofanous TG, Yuen WW. 1997. On the regimes of premixing. *Proc. Org. Econ. Coop. Dev./Comm. Saf. Nucl. Install. Spec. Meet. FCI, Tokai-mura, Japan,* ed. M Akiyama et al. JAERI-Tokai-mura, pp. 167–204
63. Duplat F, Berthoud G, Hamon M. 1997. Recent results on the Billeau premixing experiment using cold and hot spheres (2200 K) and comparison with MC3D calculations. *Proc. Adv. Reactor Safety '97 Meet. Orlando,* Vol 1, pp. 529–40
64. Meyer L. 1997. QUEOS, an experimental investigation of the premixing phase with hot spheres. *Proc. Org. Econ. Coop. Dev./Comm. Saf. Nucl. Install. Spec. Meet. FCI, Tokai-Mura, Japan,* pp. 155–56
65. Berthoud G, Pion A. 1986. Destabilization of the vapor film when a hot liquid contacts a refrigerant: application to the sodium-water reaction. *Proc. Int. Conf. Sci. Technol. Fast React. Saf., Guernsey,* pp. 399–404. British Nuclear Energy Society, London
66. Magallon D, Huhtiniemi I, Hohmann H. 1997. Lessons learnt from FARO/TERMOS corium melt quenching experiments. *Proc. Org. Econ. Coop. Dev./Comm. Saf. Nucl. Install. Spec. Meet. FCI, Tokai-mura, Japan,* pp. 431–47
67. Ando M, Caldarola L. 1982. Triggered fragmentation experiment at KFK. *Proc. Inf. Exch. Meet. Post Accid. Debris Cooling, Karlsruhe,* F2K, Karlsruhe
68. Kim B. 1985. Heat transfer and fluid flow aspects of small scale single droplet FCIS. PhD thesis, Univ. Wisc., Madison
69. Ochiai M, Bankoff SG. 1976. Liquid-liquid contact in vapor explosion. *Proc. ANS/ENS* Proc. ANS/ENS lub. Meeting on Fast Reactor Safety, 5–8 Oct. Chicago, Vol 4, pp. 1843–51
70. Tan MJ, Bankoff SG. 1981. On the fragmentation of drops. *J. Fluid Mech.* 108:109–14
71. Burger M, Carachalios C, Kim DS, Unger H. 1986. Theoretical investigations on the fragmentation of drops of melt with respect to the description of thermal detonations and their application in the code FRADEMO, *Rep. 10660.* Comm. Eur. Commun. Brussels
72. Chen X, Yuen WW, Theofanous TG. 1995. On the constitutive description of the micro interaction concept in steam explosion. *Proc. Nuclear Reactor Thermal Hydraulics 5, Saratoga Springs,* Vol. 1, pp. 1586–1606
73. Baines M. 1979. Hydrodynamic fragmentation in a dense dispersion. *Proc. Comm. Saf. Nucl. Install. Spec. Meet. FCI Nucl. React. Saf., 4th, Bournemouth,* Vol. 1, pp. 90–111. UKAEA-AEE-Winfrith
74. Carachalios C, Burger M, Unger H. 1983. A transient two phase model to describe thermal detonations based on hydrodynamic fragmentation. *Proc. Int. Meet. LWR Severe Accid. Eval., Cambridge, MA, paper TS 6-8 1-8.*
75. Theofanous TG, Saito M, Efthimiadas T. 1979. The role of hydrodynamic fragmentation in FCI. *Proc. Comm. Saf. Nucl. Install. Spec. Meet. FCI Nucl. React. Saf., Bournemouth,* Vol. 1, pp. 112. UKAEA-AEE-Winfrith
76. Yuen WW, Chen X, Theofanous TG. 1992. On the fundamental microinteractions that support the propagation of a S.E. *Proc. NURETH, 5th, Salt Lake City.* pp. 627–636
77. Chen X, Luo R, Yuen WW, Theofanous TG. 1997. Experimental simulation on of microinteractions in large scale explosions. *Proc. Org. Econ. Coop. Dev./Comm. Saf. Nucl. Install. Spec. Meet. FCI, Tokai-mura, Japan,* Vol 1, pp. 364–90
78. Saied Ahmad S. 1995. *Experiments zur Tropfenfragmentation in Wasserströmungen.* Stuttgart: Univ. Stuttgart

79. Yang JW, Bankoff SG. 1987. Solidification effects on the fragmentation of molten metal drops behind a pressure shock wave. *J. Heat Transf.* 109:226–31
80. Board SJ, Duffey RB, Farmer CL. 1972. A non equilibrium analysis of thermal explosions, *Cent. Elect. Gener. Board Rep. RD/B/N 2186.* Berkeley Nuclear Laboratories.
81. Board SJ, Duffey RB, Farmer CL, Poole DH. 1973. The analysis of metal water explosions. *Nucl. Sci. Eng.* 52:433–38
82. Baines M. 1984. Preliminary measurements of steam explosion work yields in a constrained system. *Int. Chem. Eng. Symp. Ser.* 86:97–108
83. Yuen WW, Theofanous TG. 1993. The prediction of 2D thermal detonations and resulting damage potential. *Proc. Comm. Saf. Nucl. Install. Spec. Meet. FCI,* Santa Barbara, pp. 233–50
84. Berthoud G, Brayer C. 1997. First vapor explosion calculations performed with the MC3D code. *Proc. Comm. Saf. Nucl. Install. Spec. Meet. FCI, Tokai-mura, Japan,* Vol 1, pp. 391–409
85. Corradini M, Tang J. 1993. Modeling on the complete process of 1D vapor explosions. *Proc. Comm. Saf. Nucl. Install. Spec. Meet. FCI,* Santa Barbara, pp. 204–17, NUREG/CP-0027
86. Inoue A. 1982. Study on transient heat transfer of film boiling due to arrival of a pressure pulse. *Proc. Int. Heat Transf. Conf., 7th, Munich,* Vol. 4, FB 39, pp. 403–408
87. Derewnicki KP, Hall WB. 1982. Homogeneous nucleation in transient boiling. *Proc. Int. Heat Transf. Conf., 7th, Munich* Vol. 4, PB 2, pp. 9–14
88. Honda H, Takamatsu H, Yamashiru H. 1993. Heat transfer characteristics during rapid quenching of a thin wire in water. *Heat Transf. Jpn. Res.* 21(8):773–91
89. Reynolds AB, Berthoud G. 1981. Analysis of the EXCOBULLE two phase expansion tests. *Nucl. Eng. Des.* 67:83–100
90. Berthoud G. 1999. Heat transfer modeling during a thermal detonation, Communarial Energie Atomique, *Note SMTH/LM2/99-37.* (to be published in Nuclear Technology)
91. Park HS, Yoon C, Corradini ML, Bang KH. 1994. Experiments on the trigger effect for 1 D large scale vapor explosion. *Proc. Int. Conf. New Trends Nucl. Syst. Thermohydraul., Pisa,* pp. 271–80
92. Huhtiniemi I, Magallon D, Hohmann H. 1997. Results of recent KROTOS FCI tests: alumina vs corium melts. *Proc. Org. Econ. Coop. Dev./Comm. Saf. Nucl. Install. Spec. Meet. FCI, Tokai-Mura, Japan,* pp. 275–86
93. Fletcher DF, Anderson RP. 1990. A review of pressure induced propagation models of the vapor explosion process. *Prog. Nucl. Energy* 23:137–79
94. Berman M, Beck DF. 1989. Vapor explosions: multiphase detonations or deflagrations. *Proc. Int. Semin. Containment Nucl. React., 3rd, Univ. Calif. Los Angeles* (also available as Sand. Nat. Lab. Rep SAND89-1878C)
95. Fletcher DF, Theofanous TG. 1997. Heat transfer and fluid dynamic aspects of explosive melt-water interactions. *Adv. Heat Transf.* 29:129–33